UNIVERSITY OF TWENTE.

Applied Stem Cell Technologies – AST

University of Twente

Master Assignment

March 2023 – December 2023, 10 months

SEM A. STERCKEL
Biomedical Engineering Student

THE HEART-BRAIN AXIS

MODELING THE HEART-BRAIN AXIS USING INNOVATIVE ORGAN-ON-CHIP TECHNOLOGY

Commission

Chairman – Prof. Dr. Robert Passier
Daily Supervisor – Dr. Verena Schwach
Daily Supervisor – Lena Koch MSc.
Daily Supervisor – Dr. Carla Cofiño
Outer Member – Prof. Dr. Ir. Loes Segerink

ABSTRACT

The heart-brain axis represents a complex interplay between the cardiovascular and nervous systems, influencing physiological responses crucial for maintaining homeostasis. An illustrative example of this intricate connection is evident in the pathology of heart failure, where aberrant signaling between the heart and brain exacerbates the disease progression[1]. This thesis addresses the critical need to model the heart-brain axis for disease understanding, focusing on its impact on heartbeat regulation. The primary goal is to develop an innovative model utilizing human pluripotent stem cells (hPSCs) on a microfluidic chip to mimic the brain's influence on cardiac function through autonomic nervous system (ANS) cell innervation.

Key achievements of the project include successful differentiations of cardiac embryoid bodies (cEBs), brain organoids (BO), and vagal nerve-like cells from human embryonic stem cells (hESCs). Notably, a sympathetic nerve-like cell differentiation was introduced to counter vagal heartbeat regulation, presenting morphological distinctions. Additionally, project optimization involved testing cryopreservation of beating cEBs, various density seeding for different sized BOs, and simulating on-chip conditions. The microfluidic chip, designed for controlled co-culture of these components, achieved controlled cell localization and hydrostatic perfusion of all compartments. This design addressed handling challenges, improved live cell staining, and could accommodate four distinct cell type.

This comprehensive approach contributes to advancing our understanding of the heart-brain axis, providing a foundation for disease modeling and therapeutic research. The ability to control cell localization and simulate on-chip conditions offers new opportunities for studying cardiac regulation influenced by neural connections. In the future, this research paves the way for in-depth investigations into disease-specific mechanisms, personalized medicine approaches, and the development of innovative therapies targeting the heart-brain axis.

ACKNOWLEGDEMENTS

These last 10 months I really enjoyed working on the heart-brain project. Brimming with eagerness, the challenges ahead became an exciting adrenaline rush, innervating me to give this project my all. This endeavor promised not only scientific discovery but also a heartfelt connection to the intricate dance between the heart and brain.

I express my sincere appreciation to Lena Koch for her unwavering daily supervision and guidance during the differentiation processes of brain organoids (BO) and nerve cells. Her expertise and support have been instrumental in the success of these critical aspects of the project.

A heartfelt thank you to Dr. Carla Cofiño for her dedicated support and insights in matters related to cardiac embryoid bodies (cEB). Her contributions have significantly enriched the development of this research.

I extend my deepest gratitude to Dr. Verena Schwach for her continuous support throughout this academic journey. Her encouragement and assistance have been invaluable during the various phases of this project.

Special recognition goes to the entire heart-brain team for their collaborative efforts. The inclusion of a fourth cell type on the heart-brain chip is a testament to the collective commitment and collaboration of the team, without which this research would not have been possible.

I am indebted to the experts from the BIC lab for their valuable advice and engaging discussions. Their insights have played a pivotal role in shaping the direction of this research. I extend my appreciation to Johan Bomer for his generous assistance in the cleanroom, ensuring a conducive environment for the project's execution. A warm thank you to Dr. Ir. José Rivera Arbeláez for his skillful contributions to the micro milling of the molds, a critical aspect of the project that significantly contributed to its success. Special thanks to Swathi Radhakrishnan Senthilkumaran for her invaluable contribution to calcium imaging. Her expertise in this area has greatly enhanced the quality of our data and analysis.

I am grateful to Robert for providing the opportunity to undertake my assignment and for his ongoing support in current and future endeavors. I thank Loes for her willingness to participate in the examination committee, contributing to the academic rigor and evaluation of this research.

I express my gratitude to everyone who supported my presence at the university during the weekends, facilitating an environment for productive work. Lastly, I want to thank the students of the black table for their stimulating conversations and interesting talks. Your camaraderie has been a source of inspiration and “intellectual” exchange.

Each of these individuals and groups has played a unique and indispensable role in the realization of this project, and I am truly thankful for their contributions.

TABLE OF CONTENTS

INTRODUCTION

The heart-brain axis represents a dynamic and intricate connection between two vital organs, which jointly control fundamental physiological processes. While the heart serves as the body's main engine, maintaining vital blood circulation, the brain coordinates cognitive, emotional, and autonomic functions. The multidirectional communication in this axis encompasses various neural, hormonal, and biochemical pathways that synchronize cardiovascular function with neural regulation, and vice versa[2]. This phenomenon plays a role in regulating numerous physiological responses, as well as its implications in various disease states, making it an important topic in cardiovascular and neurological research[1], [2]. In the upcoming sections, we will provide a short overview of the physiology and anatomy of the heart-brain connection, contextualizing their roles in disease. Additionally, we will explore the potential applications of stem cell technology for the use in modeling this axis.

COMMUNICATION PATHWAYS OF HEART AND BRAIN

The brain innervates the heart through the autonomic nervous system (ANS), regulating cardiac function (Figure 1) [3]. The ANS is mainly divided in the stimulating sympathetic nervous system (SNS) and the relaxing parasympathetic nervous system (PSNS), also known for the “fight or flight” and “rest and digest” phenomena respectively[3]. The SNS and PSNS both originate in the central nervous system (CNS) and extent through preganglionic nerves to the peripheral nervous system[1]. The preganglionic nerves synapse with postganglionic nerves and use the neurotransmitter acetylcholine (ACh) to transduce signals[3]. The heart is innervated by these postganglionic nerves through nerve type-specific neurotransmitter release which bind to the postsynaptic receptors of the heart[2].

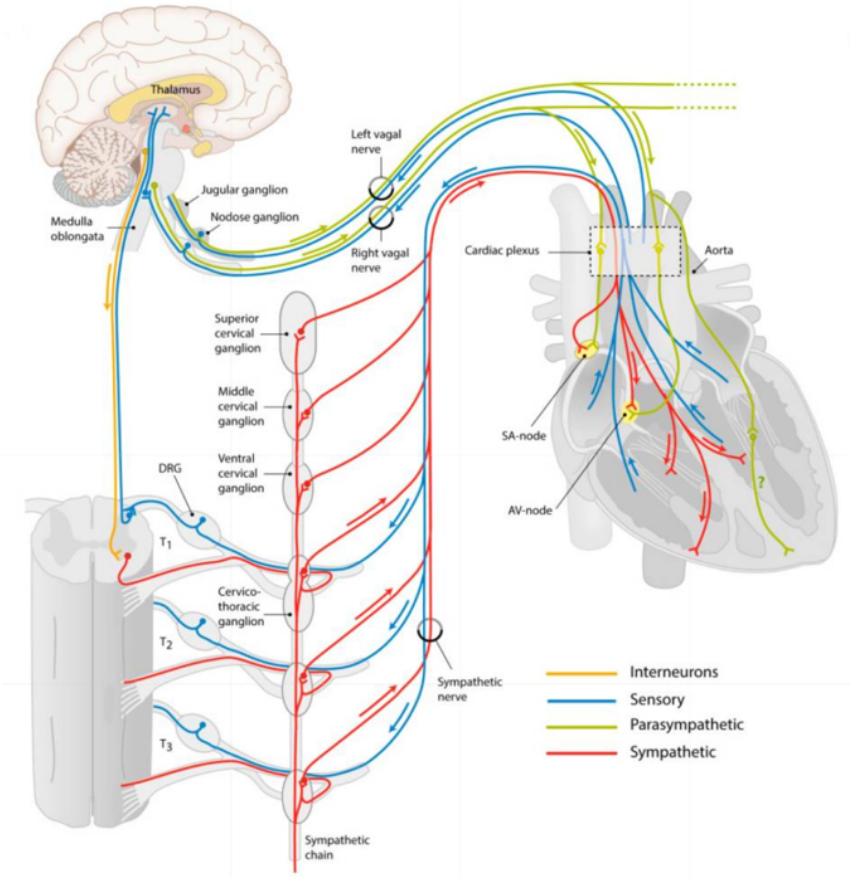

Figure 1: Schematic overview of the cardiac innervation. The autonomic nervous system sprouting from the spinal cord via the sympathetic neurons (red) and from the brain stem via the parasympathetic neurons (green). Afferent sensory neurons (blue) give feedback on to the central nervous system and interneurons (yellow) connecting the higher central nervous system with the autonomic nervous system.[3]

The preganglionic nerves of the SNS project from the thoracic and lumbar spinal cord towards the sympathetic ganglia where they forward the signal to the postganglionic nerves[3]. The sympathetic postganglionic nerves innervate the sinoatrial node, the atrioventricular node, and the ventricular cardiomyocytes (CM) in the heart[1]. Different from the sympathetic preganglionic neurons, the sympathetic postganglionic neurons' main neurotransmitter is norepinephrine (NE)[4]. NE binds to the adrenergic receptors of the target tissue, which in the developing neonatal hearts consist of α1-, β1- and β2-adrenergic receptors and in adult hearts mainly consist of β1-adrenergic receptors[1]. Activation of said adrenergic receptors leads to an increase in inotropy (contractility), chronotropy (beating frequency), dromotropy (conduction velocity), and lusitropy (relaxation) with a result of higher cardiac output[5].

For the PSNS, the heart is predominantly innervated through the vagus nerve projecting from the medulla oblongata and finding connection with the parasympathetic postganglionic neurons in the cardiac plexus[3]. The parasympathetic postganglionic neurons use ACh as their main neurotransmitter. The vagus nerve innervates the sinoatrial node and the atrioventricular nerve, however, whether the vagus nerve innervates the ventricular CM requires further research[1], [3]. ACh acts on the cholinergic M_2 muscarinic receptors of the target tissue, which in term has downregulating effects on the inotropy, chronotropy, dromotropy, and lusitropy[4], [5].

To regulate and maintain homeostasis through cardiac functioning the CNS needs feedback from a variety of afferent neurons[6]. Feedback on the blood pressure in the aortic arch and the carotid sinuses is provided by the baroreceptors[2]. When arterial blood pressure decreases, the baroreceptors firing rate decreases towards the CNS, which result in a reflex increasing sympathetic activity and decreasing parasympathetic activity[2]. Various feedback mechanisms exist through this neural control of the cardiovascular system, for example regulating oxygen concentrations, body temperature, osmotic balance, and patterns in respiratory activity[6]. The current knowledge on the neuroregulatory pathways and the exact influences of specific higher brain regions is still very limited[7]. Direct connections between the autonomic nervous divisions and the central nervous system (CNS) are established through the medulla oblongata, whereas indirect connections are postulated to exist with the pons, hypothalamus, amygdala, hippocampus, cortex, midbrain, and thalamus[6], [7].

DISEASES OF THE HEART – BRAIN AXIS

The intricate interplay between the ANS and the brain plays a pivotal role in the regulation of heart function, but also heart function can play a vital role in the functioning of the brain[2]. Disruptions in this dynamic relationship are associated with various diseases[2]. It has been estimated that 22% of the ischemic stroke cases are related to atrial fibrillations[8]. Exact mechanisms are not yet known, however, it is theorized that the brain sends out erratic electrical signals when a stroke occurs, disrupting the heart's heartbeat and inducing atrial fibrillations[9]. Another theory for this high prevalence is that atrial fibrillations cause blood pooling and blood clots, potentially embolizing the brain, causing ischemic stroke[8]. The discourse highlights the importance of the fundamental research to this complex axis.

Stress, a prevalent factor in modern life, contributes to the development of heart disease through the sympathetic stimulation orchestrated by the ANS[6]. Chronic stress activates the sympathetic nervous system, prompting the release of stress hormones like cortisol and adrenaline[10]. This heightened sympathetic activity elevates heart rate, blood pressure, and promotes inflammation, collectively fostering an environment conducive to cardiovascular disorders[10], [11]. Over time, this sustained stress response can lead to the development or exacerbation of conditions such as hypertension, atherosclerosis, and myocardial infarction, exemplifying the intricate relationship between psychological stress, the ANS, and cardiovascular disease[11], [12]

Numerous other disorders are intricately connected to the heart-brain axis. Alzheimer's, a neurodegenerative disorder characterized by cognitive decline, has been shown to affect the ANS, leading to dysregulation of heart rate variability[13]. Diabetes mellitus, for instance, can impact the autonomic control of the heart through denervation of the cardiac tissue, leading to cardiovascular complications[14]. Additionally, certain psychiatric disorders, such as depression and anxiety, are associated with an increased risk of heart disease, further highlighting the bidirectional relationship between mental health and cardiovascular well-being[12], [15]. These

intricate connections emphasize the importance of understanding and managing diseases related to the heart-brain axis.

STEM CELL TECHNOLOGIES FOR MODELLING HEART AND BRAIN

In the current age of developmental biology, human pluripotent stem cells (hPSCs) are considered a potent tool in disease modeling, offering a wide range of approaches to understand complex human pathologies[16]. hPSCs can differentiate into various cell types, recapitulating human tissues and organs in terms of function, 3D tissue structure, cell type composition and even organ to organ interaction[16]. Concurrently, organ-on-a-chip technology allows for precise control of the physiological and architectural microenvironment opening doors to advanced and innovative hPSC models[17]. These two technologies are combined in this thesis for a bottom-up development of the heart-brain axis-on-a-chip.

High-throughput differentiation protocols using embryoid bodies are often used for the formation of 3D tissues[18]. As such they have also been used for the differentiation of cardiac embryoid bodies (cEBs) with either ventricular or atrial characteristics[19]. Together with genome editing techniques, stem cell differentiations can be aided to select for successful differentiations based on specific gene expression or can be used to image intrinsic cell dynamics[20], [21]. Besides cEBs, other 3D tissues optimized for functional characterization have been developed, for example engineered heart tissues for improved contractile strength quantification[22].

When trying to model the complexity of organs, the self-organization of hPSCs becomes a great advantage in recapitulating this complexity[16]. The sheer complexity of brains thus makes it an interesting organ to model via stem cell technologies. Brain organoids (BOs) can be differentiated towards specific regions of the brain like the hippocampus, hypothalamus, forebrain, and others[23]. To study the interactions of different brain regions, assembloids can also be formed[23]. Differentiations towards specific neuronal lineages have been characterized by the expression of enzymes used in the synthesis of neurotransmitters[24], [25]. hPSC-derived neurons were found to propagate Ca^{2+} through cell bodies upon chemical stimulation.

Nonseparated cocultures of hPSC-derived neurons and hPSC-derived cardiomyocytes have been reported in literature showing NE secretion upon activation[26]. However, this model does not allow for selective stimulation or selective evaluation of cells due to there being no restrictions on the cell localization. A model using rat primary cells showed the modulating effect of sympathetic and parasympathetic neurons on cardiomyocyte activity[27]. The model used innovative micro-fabrication techniques to separate cultures while allowing axonal connections. The development a hPSC based model to recapitulate the cardiac innervation and the interaction with the brain is needed for complex disease modeling. The model should however allow for techniques with selective stimulation and selective evaluation of cells to help uncover these intricate connections.

PILOT DESIGN HEART – BRAIN AXIS

Piloting work on the heart-brain axis-on-a-chip within the research group of Applied Stem Cell Technologies has been done by Lena Koch and Carla Cofiño. A small summary on this unpublished work is presented in this chapter to help understand design choices and opportunities for improvement.

The initial design had a 6 mm long channel which was used for the culture of vagus nerve like cells (see Figure 2). On either side were spaces for 3D cultures of either heart cells or of brain cells. In-between the 3D cultures and the vagus nerve like cells, microchannels were designed with a length of 150 µm and a width and height of 10 µm. The microchannels were theorized to localize vagus nerve like cells in the middle channel during seeding, while allowing for the growth of neurites through the slits towards the 3D cultures. The chip was designed so the cultures could be cared for via the use of regular and custom cut pipette tips.

Fluorescent images of the chip show vagus nerve like cells far into the spaces of the 3D cultures. Mistakes in the design with openings larger than 10 µm in-between the nerve channel and the 3D culture spaces were the reason for this unexpected localization of cultures. High resolution fluorescent images of potential cell to cell connections showed direct contact between the vagus nerve like cells and the 3D cultures (see Supplementary Figure 1).

During the media refreshments of the cultures some complications occurred for example, the removal and addition of pipette tips for media refreshments could cause chips to detach from the substrate. Next, handling of the pipette tips in the 3D culture spaces could cause the 3D cultures to be disturbed or even accidentally removed from the chip. Another complication during culture was that the 3D cardiac cultures stopped beating after a few days on chip. A hypothetical reasoning for this occurrence was that the 3D cultures were maintained in a space with a too low nutrient concentration since the fresh media was designed to diffuse from the pipette tip on top to the 3D culture, potentially causing diffusion limits to be reached. When trying to stain the chips for subsequent calcium imaging the chips experienced problems with a too low intensity of calcium sensitive dye being reached in the chip and upon expected excitation of the vagus nerve like cells, no increase in intensity was detected. Potentially only low concentrations of the dye and excitation solution were reached due to diffusion limits in the chip.

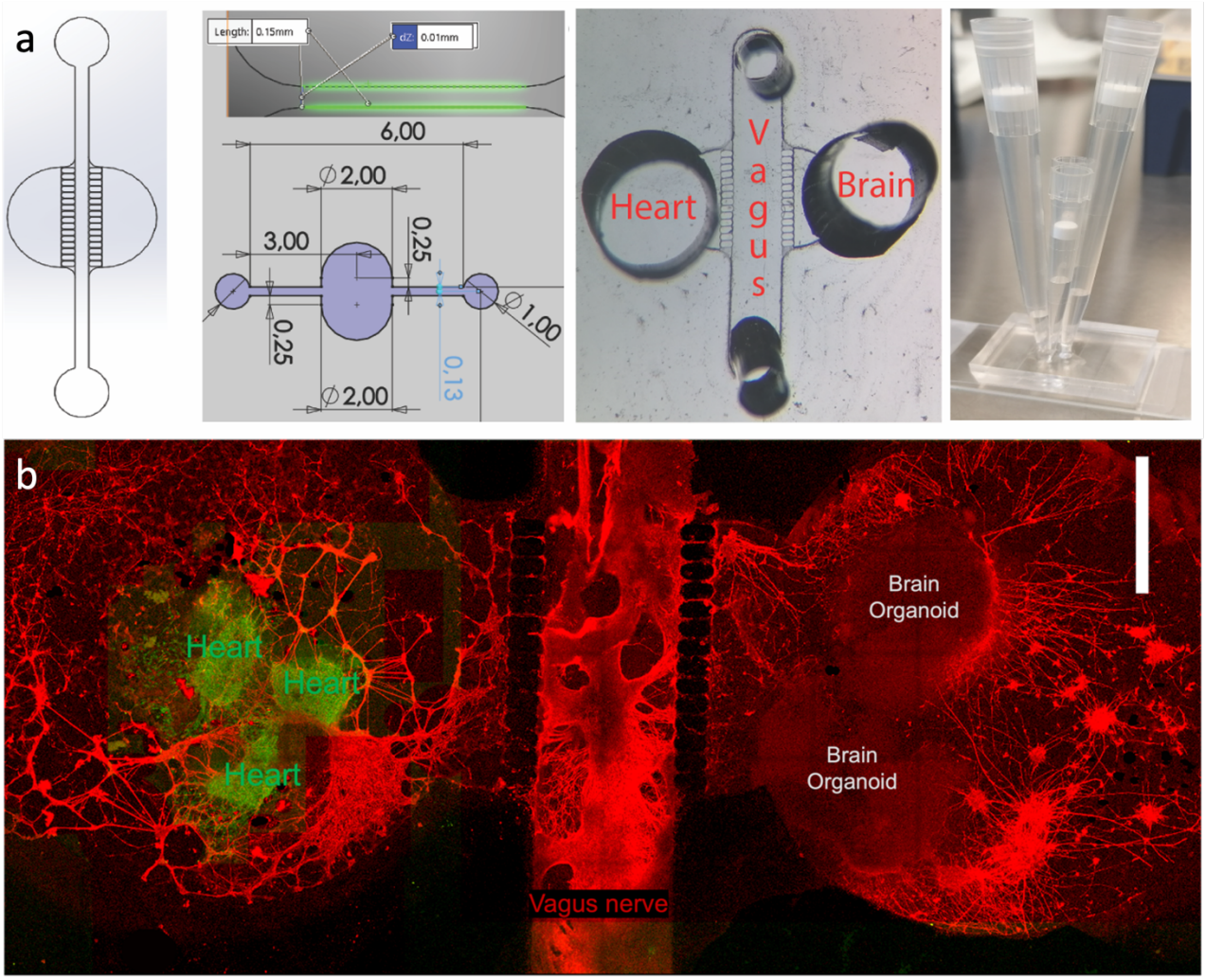

Figure 2: **Previous work on the heart-brain axis on chip within AST.** a) The general design choices and dimensions with real life pictures and pipette tip setup of the microfluidic chip. b) Fluorescent images showing three different cultures on chip with vagus nerve like cells (red), 3D cardiac cultures (green), and brain organoids depicted. (scalebar = 1000µm)

THESIS DEFINITION

This thesis is based on the need for a way to model the intrinsic axis between the brain and the heart for disease modelling. The aim of the thesis is thus to develop towards a model which mimics the effect of the brain on heartbeat regulation via the innervation of autonomic nervous cells using hPSCs on a microfluidic chip. To achieve this goal, some subgoals are defined based on previous progress within the project and in the field.

First, the different cell differentiations needed to mimic the effect of the brain on heartbeat regulation are to be differentiated from hPSCs. Already up and running protocols for cEB, BO, and vagal nerve differentiations within AST are present[19], [24], [28]. To include a counter effect on vagal heartbeat regulation, a hPSC towards sympathetic nerve like cell differentiation will be developed. This will be done through adaptation and characterization of a sympathetic nerve differentiation found in literature[25].

Next, biological research supporting the process optimization to produce the model was performed. Exploration was made into the use of different seeding densities for the BOs to obtain different sized BOs. Cryopreservation and thawing of cEBs was performed to investigate possibilities for storing 3D differentiated cultures. And lastly, nervous cell morphology and neurite formation during the nervous cell maturation stage was observed under different exposure levels to cardiomyocyte maintenance media to simulate culture conditions on the microfluidic chip.

Third, a microfluidic chip for the controlled co-culture of hPSC derived cEB, BOs, and nerve cells will be further expanded upon and optimized based on previous versions of the heart-brain axis chips from AST. The new microfluidic chip will allow for the culture of two separate types of nervous cells. More control on the localization of the different cell cultures will be obtained. Further complications of previous versions with handling causing detachment of either chips and/or cultures will be tackled while also improving nutrient availability.

Lastly, the different cell models will be incorporated in the microfluidic chip for maturation and subsequent analysis to assess the connections and interaction between the cultures. Through immunostainings direct contact between nervous cells and cardiac cells will be identified. The interaction from nervous cells towards the 3D cell culture will be imaged through a calcium sensitive dye.

METHODS

See Supplementary Methods for detailed methods and media configurations and see Supplementary Materials for a material list with manufacturer details and catalog numbers.

HESC PASSAGING

The DRRAGN (NKX2.5$^{eGFP/+}$-ACTN2$^{mRuby/+}$) hESCs were maintained in undifferentiated state on a vitronectin coating with Essential 8 (E8) stem cell medium with E8 supplements medium. The hESCs were passaged twice a week with EDTA.

DIFFERENTIATION OF AUTONOMIC NERVOUS CELLS

HESCs were seeded on a Matrigel coating in E8 media with 10µM Y-27632. Next day neural crest induction stage was initiated, and media was replaced with Knockout Serum Replacement (KSR) medium (Table S1) supplemented with 10µM SB421542 and 1µM or 0.1µM (for vagal or sympathetic differentiation respectively) LDN193189. Every second day media was replaced according to the neural crest induction stage scheme (Table S3). Base media transitioned from KSR medium to N2 medium (Table S2) in increments with supplements 3µM CHIR99021 and 1µM Retinoic Acid (RA) being added on day 2 and day 6, respectively. On day 12 cells were disassociated with EDTA and seeded on an anti-adherence rinsing solution coating in Neural Precursor induction (NPi) (Table S4) medium supplemented with 10ng/ml FGF2 and 3µM CHIR99021 for a spheroid culture. Media was refreshed every second day and on day 15 or 18 spheroids were disassociated with EDTA (Invitrogen, cat. no. 15575-038) for subsequent seeding on 15µg/ml Poly-L Ornithine / 2µg/ml Laminin-1 / 2µg/ml Fibronectin coated substrates with Autonomic Nervous System (ANS) medium (Table S5) supplemented with either only 25ng/ml GDNF or 0.2mM dbcAMP, 25ng/ml BDNF, 25ng/ml NGF, 25ng/ml GDNF, and 0.125µM RA for a vagal or sympathetic differentiation respectively. Half of the media was aspirated and refreshed every couple of days.

SH-SY5Y PASSAGING AND DIFFERENTIATION

SH-SY5Y cells were maintained in their corresponding maintenance medium (Table S6) in cell culture flasks. The cells were passaged twice a week with 0.05% Trypsin and reseeded in medium with a 1:2 ratio of conditioned and fresh media. For differentiation the cells were seeded on 15µg/ml Poly-L-Lysine / 2µgml Laminin-1 coating in 1% FBS containing maintenance medium supplemented with either 10 µM RA or 1 mM dbcAMP. Media for differentiation was refreshed every other day and cells were fixed either on day 4 or day 7 of differentiation.

DIFFERENTIATION OF CARDIAC EMBRYOID BODIES

HESCs were added to E8 media with 10µM Y-27632 and 400µg/ml Poly-(Vinyl-Alcohol) (PVA), and 5x10^3 cells per 50 µL were seeded into V-shaped 96 wells to form EBs overnight. The next day the EBs were washed with 50 µL of BPEL (Table S7) and BPEL was aspirated with a multi-channel pipette. Immediately after 50 µl of cardiac mesoderm induction medium (Table S8) was added and cells were incubated for about 3 days. At day 3, 7, and 10 of differentiation media was refreshed with 100 µl plain BPEL. On day 14 media was switched to Cardiomyocyte Maintenance (CM) media (Table S9).

DIFFERENTIATION OF BRAIN ORGANOIDS

HESCs were added to Essential 6 (E6) media with 10µM Y-27632 and 400µg/ml PVA, and were seeded into V-shaped 96 wells in 150 µl to form EBs overnight. Next day media was changed to E6 supplemented with 2µM XAV939, 10µM SB421542, and 500nM LDN193189. Media was refreshed every day until EB embedding on day 8. Embedding of the EBs was performed by sandwiching one EB between two layers of Matrigel (growth factor reduced) in custom dimpled parafilm sheets and letting the Matrigel solidify for 20 minutes. The hardened Matrigel domes were added on a anti adherence rinsing solution coating in Neural Induction Media (NIM) with supplements 3µM CHIR99021 and 0.5ng/ml BMP4 (Table S10). Media was refreshed after 2 days and was changed to Brain Organoid Maintenance Media (BOMM) (Table S11) on day 12 of differentiation. Cultures were partly refreshed every 3-4 days.

FABRICATION OF CHIP MOLDS AND PDMS CHIPS

PMMA mold designs and milling paths were created using Solidworks software (Dassault Systemes, France). Using a Datron Neo (Datron, Germany) with 200 µm and 100 µm drill bits, molds were micromilled into PMMA to create the master mold.

Photomask designs for SU-8 molds were created in Clewin5 software (WieWeb software, The Netherlands) and chromium coated-coated quartz photomasks were produced by NanoLabNL. The SU-8 25 photoresist was spin-coated on a <100> OSP, P type, 100mm silicon wafer to obtain a 10 or 15 µm thick layer. Subsequently the wafer was pre-exposure baked and exposed to UV light through the photomasks according to manufacturer's specifications. To obtain wider slits a 40% longer exposure time was used. SU-8 100 photoresist was spun on top to obtain a 200 µm thick layer, pre-exposure baked, exposed with UV light, post-exposure baked, developed with RER600, and hard baked according to manufacturer's specifications. The resulting master mold was treated with a vapor phase of FDTS.

Polydimethylsiloxane (PDMS) mixtures were made (10:1 w/w ratio of Sylgard-184 base:curing agent) and stored at -20°C until further use. PDMS was poured on the molds and left in a vacuum of -0.08 Pa for 1 hour. Mixtures were incubated at 65°C for a minimum of 3 hours to harden and afterwards reservoirs and holes were created with 2.5- and 5-mm diameter biopsy punchers. PDMS chips were bonded to glass through oxygen plasma treatment with CUTE (Femto Science, South Korea).

Smoothcast molds were made by mixing the components according to manufacturer's specifications, pouring the mixture onto unpunched PDMS chips, and baking at 65°C overnight.

CHIP MOLD AND PDMS CHIP CHARACTERIZATION

To estimate heights of SU-8 molds after development, a Dektak 150 Surface Profiler (Veeco Instruments, USA) was used on the SU-8 100 channels and the SU-8 25 resolution markers for the estimated height of the general channels and microchannel respectively. Widths were estimated by manual measurement on the microchannels in images.

To estimate the mixing of the different maturation media on chip during culture, two different color dyes – red and blue - were added to the autonomic nervous cell reservoirs and the 3D cell culture reservoirs and left on a rocker at an angle of 5 degrees rocking every 30 seconds for about 72 hours. A calibration curve for color dye mixes with increments of 10% were made and compared with the samples taken from the reservoirs using a Varioskan LUX spectrometer (Thermo Fisher Scientific, USA).

CELL CULTURE ON CHIP

Right after chip bonding, the chips were coated with on 15µg/ml Poly-L Ornithine / 2µg/ml Laminin-1 / 2µg/ml Fibronectin. Before seeding, the chip was aspirated and left to dry for 10 minutes. Disassociated neural progenitor cells were seeded by adding 10 µl medium to one reservoir and 100 µl cell suspension to the other connected reservoir. 3D cultures were seeded by first adding the corresponding maintenance media to the reservoirs and then adding the 3D cultures via the chamber opening on top. Two cEBs or one BO was seeded per culture chamber and BOs had the Matrigel domes removed prior to seeding. Chips were placed on a rocker at an angle of 5 degrees rocking every 30 seconds.

CALCIUM IMAGING OF CHIPS

Staining solutions were prepared with 5 µM of Fluo8-AM in HBSS. Samples were incubated in the staining solutions for 30 minutes at 37°C and afterwards incubated in their base media for 30 minutes before imaging. Live cell imaging was done using a Nikon Eclipse Ti2 (Nikon Instruments, Japan). Autonomic nervous cells were excited by removing the media in one reservoir and adding 50 mM of KCl solution.

IMMUNOSTAINING

Cell cultures were fixated via either a general monolayer fixation and staining protocol or via alterations on this standard protocol for optimization. For the general protocol, the culture is washed twice with PBS and incubated for 15 minutes in PBS with 4% paraformaldehyde (PFA) at RT. After fixation cultures were washed with PBS and stored in PBS with 1% penicillin/streptomycin at 4°C until further use. Samples were incubated in blocking buffer

(3% BSA in PBS) with 1% Triton X-100 at RT and subsequently incubated with the primary antibodies in blocking buffer overnight at 4°C. See Table S13 for used antibodies and dilutions. Samples were washed in washing buffer (0.1% BSA in PBS) before incubation with the secondary antibodies in blocking buffer for 1 hour at RT. Optionally, samples were incubated with DAPI in blocking buffer for 10 minutes at RT. After washing, samples were kept in washing buffer with 1% penicillin/streptomycin at 4°C until further use. Alterations on the general protocol for hESC derived nervous like cells or SH-SY5Y included the following: using prewarmed (37°C) HBSS or prewarmed PBS with 4% glutaraldehyde during prefixation washing steps; using 3% FBS instead of BSA; using TBS instead of PBS. Alterations on the general protocol for chips consisted of using fixation incubation times of 45 minutes and using twice as high of a concentration for antibody incubations. Imaging of immunostainings was done with either a EVOS FL M7000 (Thermo Fisher Scientific, USA) or a LSM880 Zeiss microscope (Zeiss, Germany).

CRYOPRESERVATION

Single cell cultures and cEBs were cryopreserved with custom cryopreservation media (Table S12). Cryovials were kept in a Mr. Frosty at -80°C overnight and the next day cryovials were stored in liquid nitrogen until further use.

For cryopreserved single cell cultures, cryovials were thawed and cell suspensions were added to their prewarmed corresponding media. Subsequently, suspensions were centrifuged, aspirated, resuspended in corresponding media, and seeded. For cryopreserved cEBs, cryovials were thawed and the cEBs were relocated in baths of their corresponding prewarmed media. After washing steps, the cEBs were placed in anti-adherence solution coated 96 V-wells with their corresponding media.

STATISTICAL ANALYSIS

Data are represented as mean ± S.D. Unless otherwise noted, differences were tested for significance using two-way analysis of variance (ANOVA). A P value less than 0.05 denoted statistical significance.

RESULTS & DISCUSSION

HESC DIFFERENTIATION INTO TWO MORPHOLOGICALLY DISTINCT NEURONAL CELL TYPES

The development of a hPSC-derived sympathetic like neuronal differentiation was needed for constructing the hPSC heart-brain axis model containing both ANS divisions. The direct comparison of sympathetic and vagal differentiation methods has not been described in terms of morphology and protein expression. Based on reports in literature, it is expected for the differentiations to differ in terms morphology and group behaviour about 4 days before the Neural Precursor induction (NPi) stage and during the maturation stage[24], [25], [29]. Sympathetic like neurons are more compact together before the NPi stage and are flatter and less grouped together during maturation. The sympathetic like neuron is characterizable by the enzyme involved in producing neurotransmitter NE, tyrosine hydroxylase (TH)[25].

The protocols used for differentiation of hESCs into either a vagal like neuronal cell type and sympathetic like neuronal cell types were adaptations from the original protocols from Fattahi or Saito-Diaz, respectively (see Figure 3)[24], [25]. The first twelve days of differentiation into neural crest like cells differed in terms of a higher LDN193189 concentration, the addition of RA, and increasing media volumes for the vagal differentiation. The higher BMP activation and subsequently SMAD inhibition through LDN193189 combined with the regulating effect on HOX gene expression by RA is expected to increase mature neuron differentiation efficiency[30]. After the Neural Precursor induction (NPi) stage, the cultures are in different maturation media with the difference in supplements being the extra addition of BDNF, NGF, dbcAMP, and RA which is expected to help guide towards a more efficient sympathetic differentiation[25], [31].

During this neural crest induction stage, both differentiations formed a dense layer of cells and around day 8 of differentiation ridges formed as expected (see Figure 3). The sympathetic differentiation formed larger ridges with a heavy pattern compared to the smaller patchwork seen in de vagal like differentiation, as expected. A size difference in spheroid formation seemed present between the conditions. Further analysis on the size distribution via ImageJ comparing the two spheroid groups showed that for vagal precursor spheroids were significantly larger than the sympathetic precursor spheroids ($p<0.001$). This difference could induce further differences since precursor spheroid size was reported to be an important factor in differentiation[29]. After replating of the cells into the different maturation media, characteristic differences in cell morphology and group behavior were seen at day 22 of differentiation similar to what was reported in literature [24], [25](see Figure 3). The sympathetic like cells showed a flatter and larger morphology compared to the vagal like cells. The vagal like cells showed a stronger tendency to cluster together. Both conditions showed clear neurite formation, characteristic for neuron differentiation. At around day 24 in both conditions confluence was reached and at day 28 clustering of cells will open spaces and neurite networks can be seen, as reported previously in neuronal differentiations[24], [25].

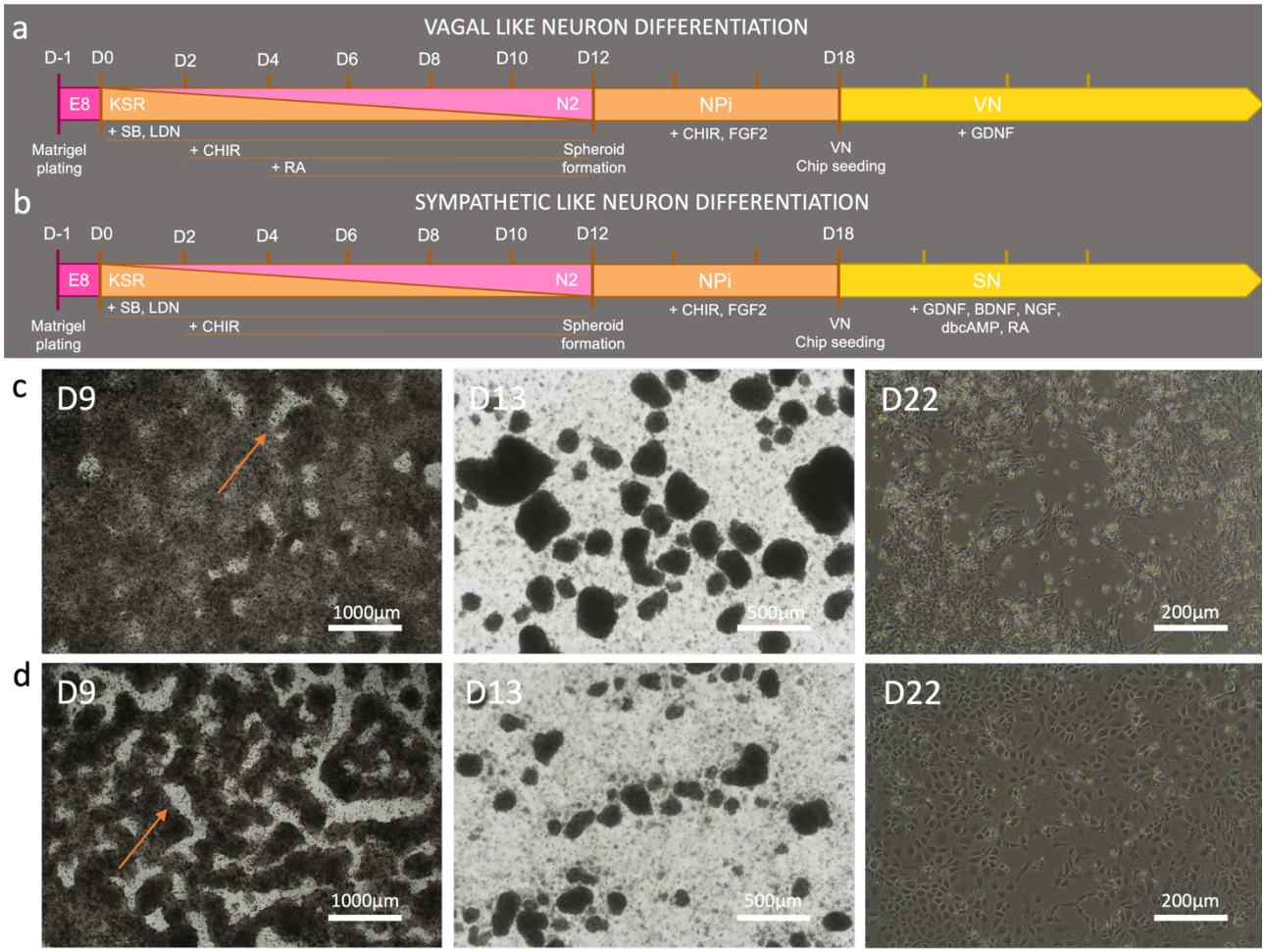

Figure 3: **Vagal like and sympathetic like neuron differentiations compared.** a,b) Schematic overview of the differentiation scheme for the lineage specific neuron. c,d) Brightfield images of the vagal (c) and sympathetic (d) cultures at the timepoints day 9, 13, and 22 of differentiation. Orange arrow indicates ridges.

Markers for mature neuron nuclei (NeuN), the neuronal cytoskeleton (B3-Tubulin), glutaminergic neurons (VGLUT), peripheral autonomic neurons (Phox2B), dopaminergic neurons (Foxa2), neural crest nuclei (Pax6), mature neurons (HuB/C/D), and a sympathetic neuron specific protein used in the formation of NE (TH) were used [24], [25]. During the staining procedure some patches of the culture detached and were washed away, thus only small amounts of sample were left for imaging. B3-Tubulin staining seemed heterogeneous, lacking in precision staining of the cytoskeleton and having inconsistent intensity (Figure 4).

The staining for mature neuronal nuclei, NeuN, showed signal on nuclei, cell bodies and neurites in both differentiations, but to a greater extent in the sympathetic differentiation. This indicated suboptimal staining of NeuN in the sympathetic cells. The immunostainings for VGLUT, Phox2B, Foxa2, Pax6, and HuB/C/D had aspecific staining and heterogeneity in signal intensity throughout conditions (see Supplementary Figure 2). The staining for TH, seemed to show a higher intensity in overall signal within the sympathetic differentiation compared to the vagal differentiation, which is as expected. However, when also taking into consideration the staining quality of the other markers, it would be useful to validate and characterize the TH staining on positive control samples before concluding a successful differentiation. According to literature differentiated SH-SY5Y cells express tyrosine hydroxylase and can be used as a positive control[32]. To improve further characterization experiments, the fixation and staining procedure should be optimized to keep cultures adherent to the substrate and to increase the signal to noise ratio.

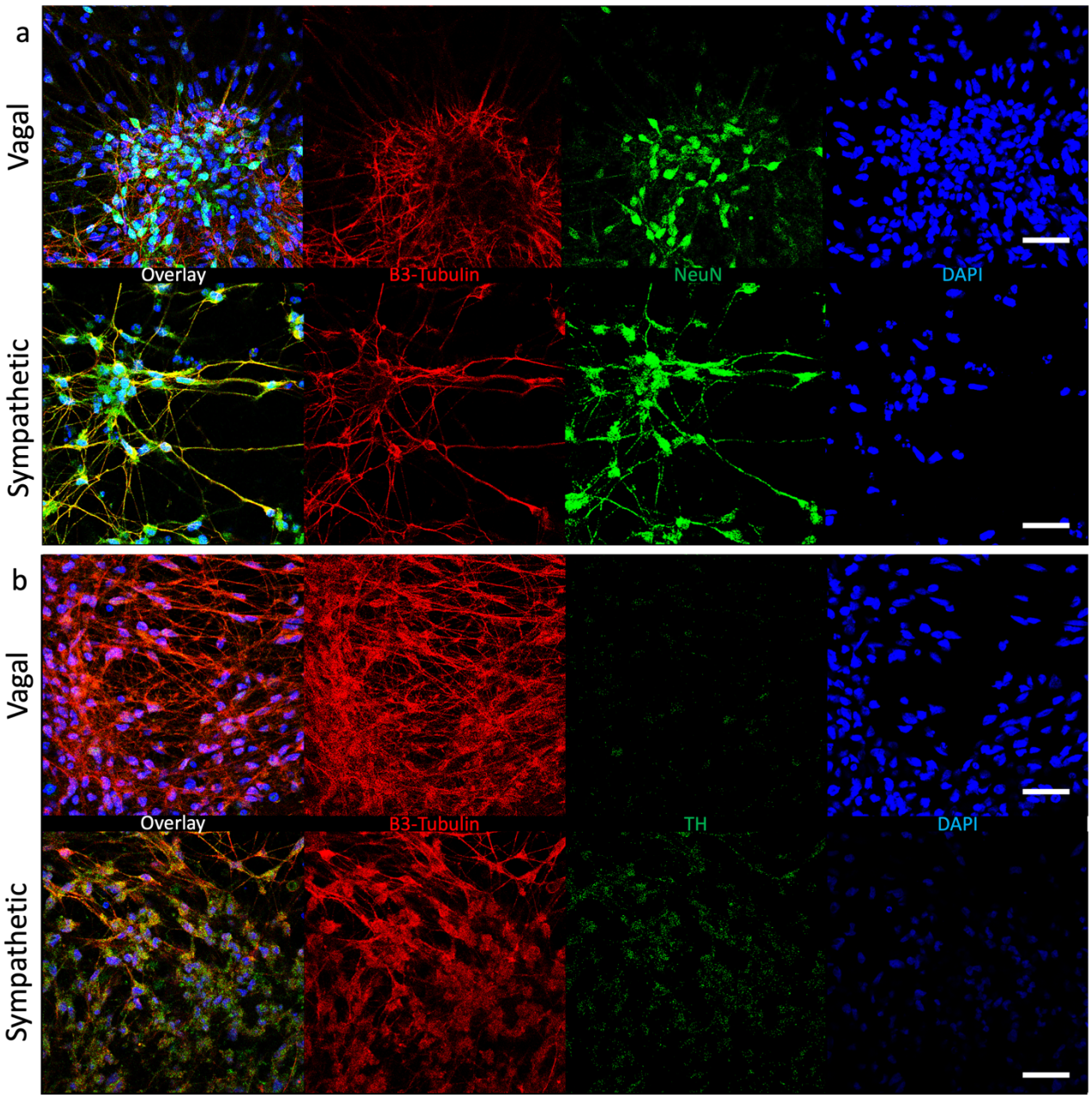

Figure 4: **Vagal and sympathetic differentiated cells at day 30.** a) Cells stained for neuronal cytoskeleton (B3-Tubulin), mature neuron nuclei (NeuN) and nuclei (DAPI). b) Cells stained for B3-Tubulin, sympathetic neurons (TH), and nuclei (DAPI). (Scalebar = 50 µm)

DOPAMINERGIC DIFFERENTIATED SH-SY5Y FAILED TO STAIN FOR TYROSINE HYDROXYLASE

A positive control for the marker TH is the dopaminergic differentiated SH-SY5Y neuroblastoma cell according to literature[32], [33]. Through exposure of the cells with 10 µM RA they are reported to form polarized elongated cells which stop replicating and grow neurites. Since SH-SY5Y cells were known within AST to be difficult to fixate and stain, multiple variations for fixation and staining were used (see Methods).

Culturing these cells with a seeding density of 10K/cm^2 in SH-SY5Y maintenance media with 10 µM RA displayed the expected morphological differences compared to the cells without RA on day 4 (Supplementary Figure 3). RA treated cells tended to cluster less than the control condition, which was also seen in literature[32], [33]. After seven days, controls formed large 3D cell aggregates, while differentiated cells started to cluster. The relatively higher proliferation of non-differentiated cells was anticipated, but the formation of extensive 3D aggregates was unexpected[32], [33]. Clustering in RA-exposed conditions appeared more pronounced than depicted in literature. These unexpected findings could be due to high cell density seeding which resulted in even higher densities being caused by undifferentiated cells. Seeding densities used in literature were lower at 4,2 K/cm^2 - 5K/cm^2[33], [34]. Using various staining protocols as described in the methods resulted in suboptimal cell retention, especially without prewarmed buffer for prefixation washing steps. Loss of almost all cells, except in the corner of wells, was observed in these conditions. Pre-fixation washing with warm buffers reduced cell loss (Supplementary Figure 3). Potential detachment of SH-SY5Y cells may be attributed to a mild cold shock during the prefixation washing, and aggregate formation might have contributed to increased cell detachment due to cell-cell attachment preference over cell-substrate attachment[35]. The few cells left in the condition exposed to RA did not have the key morphological signs of differentiation previously described. These cells were all negative for TH staining.

The experiment was repeated, but with a lower seeding density of 5K/cm^2 and a reduced FBS concentration to 1%. Changes were made to reduce proliferation and prevent high densities being reached in late timepoints. The differentiation method of exposing the cells to 1 mM dbcAMP was newly included. According to literature expression of TH is higher compared to RA treated cells and significantly expressed at day 4 of differentiation[34]. Fixation timepoints were subsequently chosen to be on day 4 and 7 of differentiation. Additionally, dbcAMP treated cells showed higher expression in MAP2, a neuron-specific cytoskeleton marker enriched in dendrites. The cells exposed to dbcAMP were reported to show less clustering and more neurite elongation, but less cell bodies elongated as with the RA exposed cells[34]. The fixation and staining method used was the variation with the prewarmed HBSS buffer as described in the methods, due to the observed improved cell retention. An analysis was performed to obtain semi-quantitative data on MAP2 expression in immunofluorescent signals, which was normalized against B3-Tubulin, a neuronal cytoskeleton marker. Regions of interest (ROIs) were randomly selected on individual cells and cell clusters. The integrated fluorescence intensity of each ROI was measured using ImageJ and normalized for area. Subsequently, the normalized MAP2 intensity was divided by the normalized B3-Tubulin intensity to determine the relative MAP2 expression.

On day 4 cells treated with RA showed morphology as expected with growth of neurites and polarized elongation of about 50% (manually counted) of the cell bodies (Figure 5)[33]. Cells exposed with dbcAMP showed neurite elongation as expected, and less than 10% (manually counted) polarized elongated cells[34]. On day 7 the cells in the experimental conditions showed slight cell clustering as expected, while the control cells had unexpectedly formed small 3D aggregates (see Supplementary Figure 5). After fixation and staining the day 7 timepoint had suboptimal cell retention. Day 4 fixation had improved cell retention in experimental conditions, with no change in confluency seen. The control condition did see a change in confluency, from 30% before to 10 – 20% after fixation and staining. It is expected that the 3D aggregates and clusters with cell-cell attachment preference over cell-substrate attachment were washed away. Immunofluorescent images show B3-Tubulin expression in all conditions and neurites in both experimental conditions (Figure 5). TH expression was not visible, contrary to expectations. MAP2 stained with the same secondary anti-body was expressed (Figure 5). Relative expression of MAP2 in the control was 0.12 ± 0.03 (n = 6), and 0.13 ± 0.02 (n = 6) in the dbcAMP treated condition. There was no significant difference in the relative expression of MAP2 between the two conditions ($p = 0.98$, $\alpha = 0.05$). This result is not in line with findings in literature, however, a more suitable method for determining protein expression was used in literature, namely western blotting with β-actin as internal control[34]. The results strongly suggest that the TH antibody used in this study may not be functional. Cells exhibiting key morphological

features indicative of differentiation were not positively stained. Consequently, it is concluded that this specific batch of TH antibody is not suitable for the characterization of sympathetic differentiated hESCs.

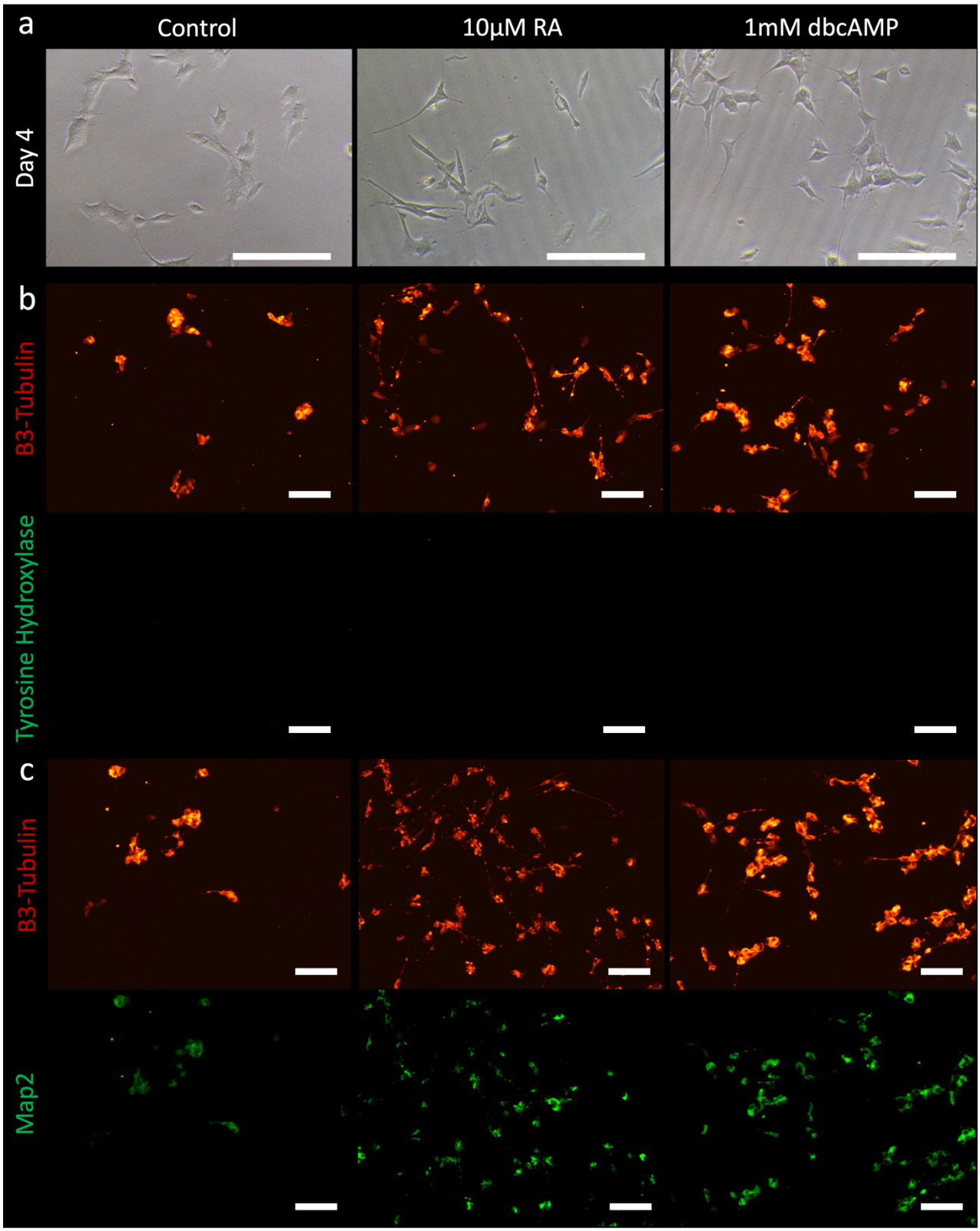

Figure 5: **Undifferentiated SH-SY5Y cells compared to dopaminergic differentiated SH-SY5Y cells via either retinoic acid (RA) stimulation or dbcAMP stimulation.** a) Bright-field images show differences in morphology between the conditions at day 4. b) Staining of day 4 samples for neuronal cytoskeleton marker (B3-tubulin) and tyrosine hydroxylase show no signal for tyrosine hydroxylase antibody. C) Staining of day 4 samples for B3-Tubulin and neuronal dendritic cytoskeleton marker (Map2). (scalebar = 50µm)

CRYOPRESERVATION OF BEATING CARDIAC EMBRYOID BODIES

Previous studies have shown that cryopreservation of hPSC-derived cardiomyocytes does not compromise molecular, physiological, and mechanical properties[36]. An investigation was conducted to assess the cryopreservation feasibility of beating cardiac embryoid bodies (cEBs) for future use. This would allow to simplify the planning of multiple differentiations for on-chip seeding within a specific timeframe. Cryopreservation of cEBs on day 12, two days before their intended use in downstream applications according to the standard differentiation protocol (Figure 6), aimed to facilitate the recovery of cEBs before further use. In anticipation of the standard differentiation's medium switch from BPEL to CM media at day 14, an experimental condition was added. This experimental condition involved switching to CM media before cryopreservation to avoid disturbing the cEBs with a media switch during their recovery. To further help cEBs recovery it was experimented with the addition of rock inhibitor[37]. Successful cEB differentiations were expected to show a round and dense morphology with defined edges and expression of NKX2.5-GFP and ACTN2-mRuby throughout the entire cEB[19], [21]. Beating of a cEB was expected to be seen as a contraction of the entire cEB.

The hESCs successfully differentiated into beating NKX2.5-GFP and ACTN2-mRuby positive cEBs (Figure 6). Cryopreservation on day 12 using either BPEL or CM media, followed by thawing in subsequent BPEL or CM media with/without rock inhibitor, was performed. Expression of NKX2.5-GFP and mRuby-ACTN2 in cEBs at day 13, along with corresponding bright-field images, is depicted in Figure 6. Cryopreserved cEB morphology appears asymmetrical and disturbed, with undefined edges and debris compared to regular morphology. Asymmetrical bloated cEBs are characteristic of suboptimal differentiation batches (Supplementary Figure 4). Images of non-cryopreserved cEBs from the same batch would have helped assess the effect of cryopreservation. Conditions thawed in media with rock inhibitor show less debris at day 13, as expected. The cEBs thawed in BPEL showed both NKX2.5-GFP and ACTN2-mRuby expression in only parts of the cEB. This partial expression is also seen in suboptimal differentiated batches (see Supplementary Figure 6). This similarity suggests that cryopreservation was not favourable for differentiation, or the differentiation was suboptimal before cryopreservation and the state of the cEB was preserved well. Cryopreservation in CM medium shows no NKX2.5-GFP signal but maintains ACTN2-mRuby throughout, potentially indicating a detrimental effect on NKX2.5 expression. The preservation of mRuby signal could be due to the fusion with ACTN2, persisting in sarcomere structures that are found not to decay after 1 day of induced stress[38].

In Figure 6, BF images of cEBs at day 18 with corresponding expression of NKX2.5-GFP and ACTN2-mRuby are displayed. For conditions thawed in BPEL media and switched to CM media, debris around the cEB has become less compared to day 13 and the edges are more pronounced, indicating that the cEB has recovered. Asymmetry and bloated regions are indicative of a suboptimal differentiation. Similar to day 13 the NKX2.5-GFP and ACTN2-mRuby is expressed only in parts of the cEB, again indicating suboptimal differentiation. Conditions thawed in CM media showed no difference in terms of morphology at day 18 compared to day 13, but small regions of NKX2.5-GFP expression were seen. These regions also showed stronger fluorescent signal compared to other regions within the same cEB. This increase in signal implied that only a small section of the cEB has recovered. Contraction within the cEBs were seen in 50% of cEBs thawed in BPEL media (n = 12) and 40% of cEBs thawed in CM media (n = 20). However, the contraction seen in BPEL thawed cEBs was more intense (see Supplementary Figure 4), which is to be expected since NKX2.5-GFP positive cells are found in literature contract and the BPEL thawed cEBs contained larger sections of NKX2.5-GFP positive cells[39].

The results found in this experiment showed the potential for the cryopreservation of beating cEBs. More data on the characteristics of the cEBs after thawing will be necessary to determine whether these cEBs could be used for future experiments. Cell viability assays for 3D cultures and immunofluorescent staining will help visualizing structural integrity. Flow cytometry might be used to quantify different cell types and voltage/calcium sensitive dye imaging could be used to determine on electrophysiology and calcium handling within the cEB. Cryopreservation of cEBs would allow for the storage of large batches of successfully differentiated cEBs, ready to be thawed and used. In the context of the complex planning and multiple labor-intensive differentiations of the heart-brain axis models, bypassing the risk of a bad differentiation batch will help improve the efficiency of fabricating successful models. In terms of using the same cryopreservation technique on the other differentiations for the model, advances are being made within AST to achieve this.

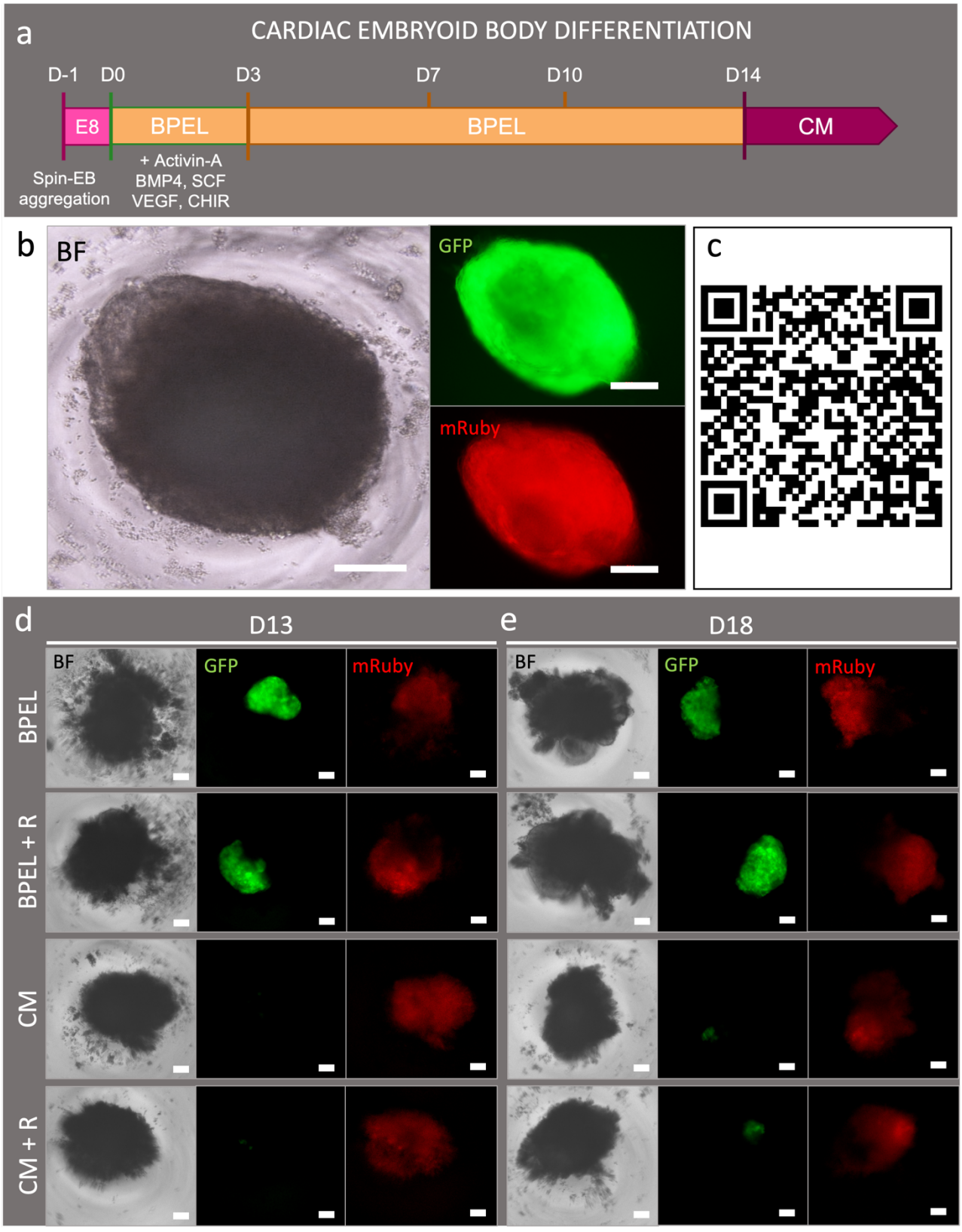

Figure 6: **HPSC-derived cardiac embryoid body (cEB) culture and cryopreservation.** a) Schematic overview of cEB differentiation scheme. b) Bright-field (BF) image and concurrent NKX2.5-GFP and ACTN2-mRuby expression of a cEB at day 18. c) QR-code to movie of beating cEBs. d,e) BF image and concurrent NKX2.5-GFP and ACTN2-mRuby expression of cryopreserved cEB at day 13 (d) or day 18 (e). Panels show cEBs thawed in either BPEL medium, BPEL medium with rock-inhibitor, CM medium, or CM medium with rock-inhibitor (top to bottom). (scalebar = 200µm)

SEEDING DENSITY DOES NOT CONTROL BRAIN ORGANOID SIZE

Smaller sized brain organoids (BOs) were needed to allow for easier seeding of brain organoids (BOs) into the relatively tight openings of the heart-brain axis chip. Since seeding density for embryoid body (EB) formation was found to affect EB size in literature, it was expected that this difference in size would persist during BO differentiation[40]. Symmetric EBs with defined edges in early development will show budding and neurite outgrowth during the neural induction stage according to literature[28]. During maturation the budding becomes less pronounced, and a complex BO is formed.

The schematic differentiation scheme used for the differentiation of hESCs towards BOs can be seen in Figure 7. The hESCs were seeded at different seeding densities, namely $5x10^3$, $7x10^3$, and $9x10^3$ per well, and spun down into EBs. The BO differentiations were imaged, and the diameter was determined with the function "Analyze Particles" in ImageJ assuming that the structures were perfectly circular.

The formation of symmetric EBs with defined edges was seen and this morphology persisted until embedding at day 8 (Figure 7). After embedding the EB seemed compacter and with less debris, which could be due to handling and compaction of Matrigel. During neural induction, distinct budding and neurite growth into the Matrigel domes, indicating presence of neuronal cells (Figure 7). The budding smoothed out during BO maturation and a dense structure remained. No differences in the morphology of the BO differentiation with different seeding densities were observed until day 12, but during maturation rougher edges were seen in the high seeding density BOs (Supplementary Figure 5). This indicates that the maturation was affected by the initial seeding density. When comparing the diameters of the BO differentiations with different initial seeding densities we see that the lower seeding densities achieve significantly smaller diameters, as previously reported (Figure 7). Smaller EBs grew larger in size, while the size of EBs of about 800 µm stayed similar, comparing day 0 to day 7. Potentially a limit on growth size of EBs exist within these conditions. No significant difference in size between seeding densities was found after Matrigel embedding. Determining diameters of BOs with strong asymmetric budding might have caused some inaccuracies. However, during later stages in differentiation where BOs were rounder this difference in diameter was again not significant.

These results show that using different initial seeding densities will not reduce matured BO size. Still, there is need for smaller BOs at the timeframe of seeding on chip (day 20 – 35), since it will allow for easier addition of BOs to the heart-brain-axis chip. Seeding EBs with an even smaller initial seeding density will cause for lower efficiency in symmetrical EB formation[40]. So, there is a limit to this strategy for improving the BO addition to the chip. Another strategy to help reduce the size of the 3D culture is by breaking down the Matrigel dome more effectively or being able to culture the BO without the Matrigel dome. Breaking the Matrigel off the BOs has its current complications in practice, with leftover Matrigel increasing the perceived BO size during handling.

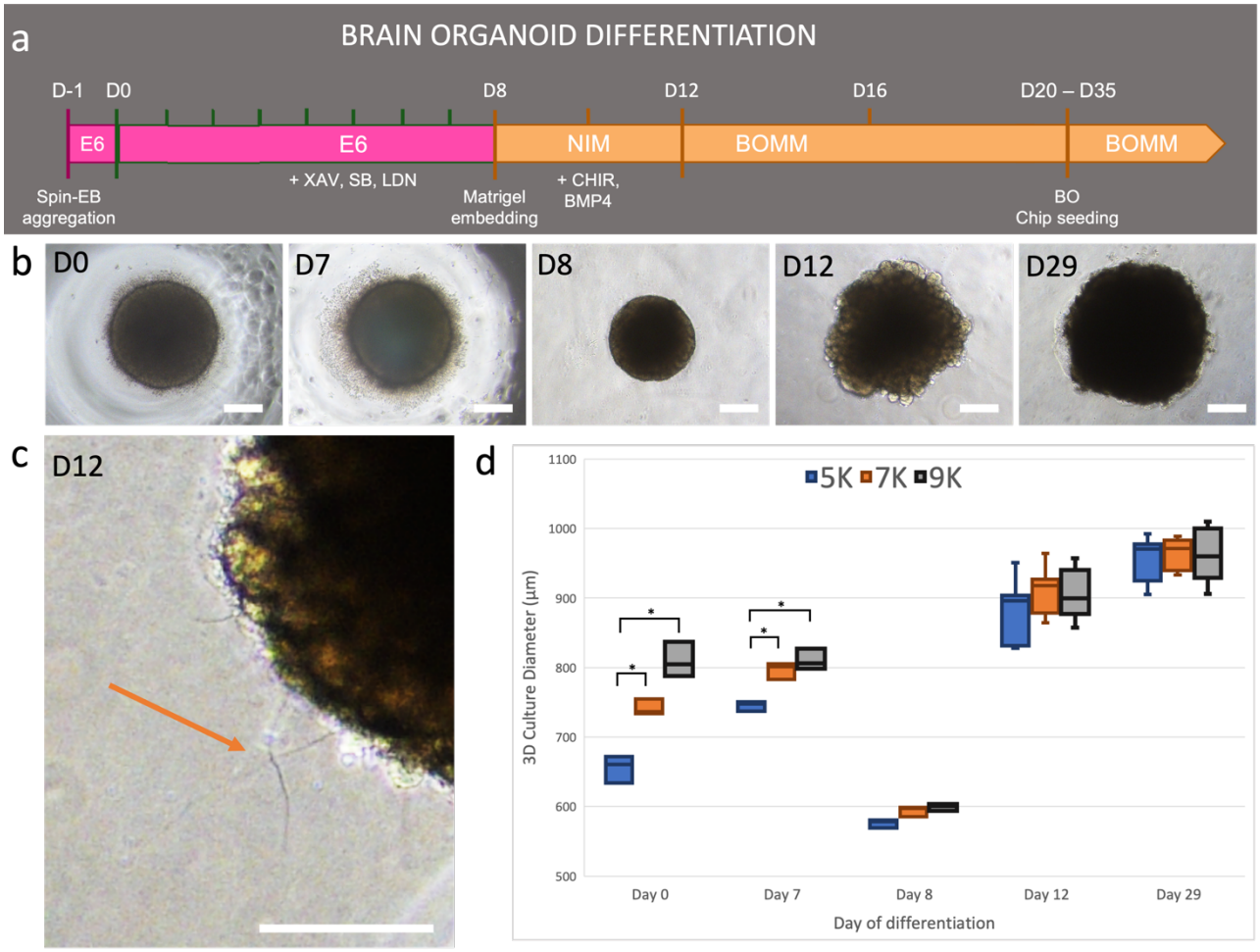

Figure 7: **Brain organoid (BO) differentiation.** a) Schematic overview of the BO differentiation. b) Bright-field images of BO differentiation at day 0, 7, 8, 12 and 29. c) A detail image of BO budding and neurite outgrowth at day 12. d) Box-plot distribution of sample diameter at different days of differentiation and at different seeding densities. Box plots include maximum, minimum, and mean values. At day 0, 7, and 8 per density 3 samples were used (n = 3) and at day 12 and 29 per density 10 samples were used (n = 10). *P<0.05. (scalebar = 250µm)

CARDIOMYOCYTE MEDIA DOES NOT OBSTRUCT NEURITE FORMATION

In the heart-brain-axis chips it is expected that neurites will grow through the microchannels to the other compartment for interaction with the 3D culture. The ability of the neurons to grow neurites will thus be essential for the connection made by the neurons with the cEB. However, these microchannels will also allow for CM media to diffuse into the nerve cell compartments, which could disturb the formation of these neurites. In this experiment neuron progenitor cells are seeded for maturation towards vagal like neurons in either pure ANS media or a 50:50 ratio of ANS media:CM media.

After 4 days of exposure to CM/ANS media neurites can be seen, and the general cell morphology does not seem to differ from the control of pure ANS (Figure 8). Both conditions had clustering and spaces opening showing neurite networks at 18 days of maturation. Neurites crossing these spaces reached lengths of 200 µm in the CM/ANS media. Quantification of neurite length or amount for a direct comparison between conditions was not performed, since the monolayer differentiation only allowed for small, arbitrary patches of open spaces with neurites present. A more controlled head-to-head comparison could be achieved in a system where cell bodies are compartmentalized, and neurites can be distinguished more effectively. The results showed proof of concept that neurite networks and long neurites can be formed in a 50:50 ratio of CM media and ANS media. This experiment, however, only shows how neurites are formed in a homogeneous mixture of ANS media and CM media. The growth of neurites against gradients of CM media are not simulated and will likely be present in the heart-brain axis chip. The influence of CM media on the efficiency of differentiation and effect on differentiation towards different neuronal lineages is another interesting topic for research. In a model where two different

neuronal lineages with different functions are attempted to be differentiated it is crucial to determine the effect of CM media on these differentiations.

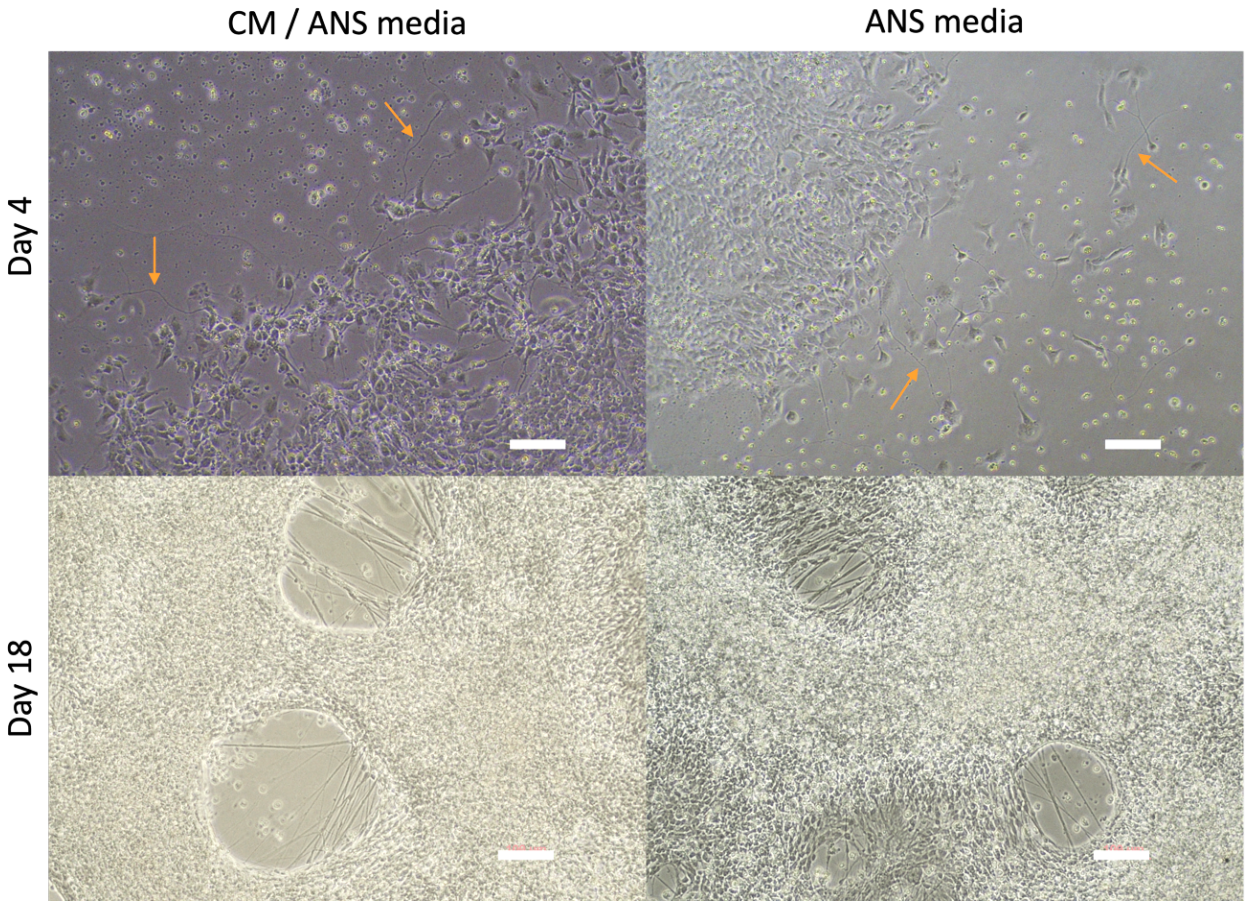

Figure 8: **Neurons exposed to either a mixture of cardiomyocyte maintenance (CM) / autonomic nervous system (ANS) media or only ANS media.** At day 4 of maturation the growth of neurites can be seen (orange arrows). At day 18 of maturation open spaces contain neurite networks with neurites longer than 200µm. (scalebar = 100µm)

HEART – BRAIN AXIS CHIP DEVELOPMENT

Initial experiments done with a pilot design for the PDMS heart-brain axis chip (from now on referred to as "chip") showed promising results for coculture of cEBs, neurons, and BOs. However, some points for further development were mentioned and are summarized below.

New designs should allow for the controlled localization of the different cell types to allow for distinguishing these cell types during characterization and analyses. An extra neuronal compartment should be designed to allow for the culturing of both sympathetic and parasympathetic neurons. Diffusion limited regions on the chip need to be perfusable, since the current chip had complications with nutrient deficiency for culturing large 3D cultures and effective live cell staining. New methods to improve chip handling and fabrication need to be developed, considering current problems with media refreshments and chip handling causing either disturbance in the cultures or detachment of the chip.

GENERATION 2.1 (G2.1)

The second-generation heart-brain axis chip (G2.1) was designed to address complications from the previous model (Figure 9). Two square compartments were designed for 3D cultures, while adjacent two longer compartments would accommodate neurons (Figure 9). Microchannels (10 µm width and height) between these compartments would enable neurite growth while preventing cell body passage during seeding [41]. Eight cylindrical reservoirs (diameter: 5 mm) store approximately 100 µl medium each in a 5 mm high chip. These reservoirs were strategically positioned so that a rocking motion along the width of the chip would lead to a build-up in hydrostatic pressure in between two coupled reservoirs. This pressure, in turn, would cause the medium to flow and perfuse the compartment. Neurons could be seeded into their compartments through this mechanism, but 3D cultures use a top opening in the compartment for planting. Integrated reservoirs simplify fabrication and handling, eliminating the need for custom pipette tips and enabling non-disruptive media aspiration. Micro milling in PMMA would be used to produce re-usable molds for PDMS chip fabrication.

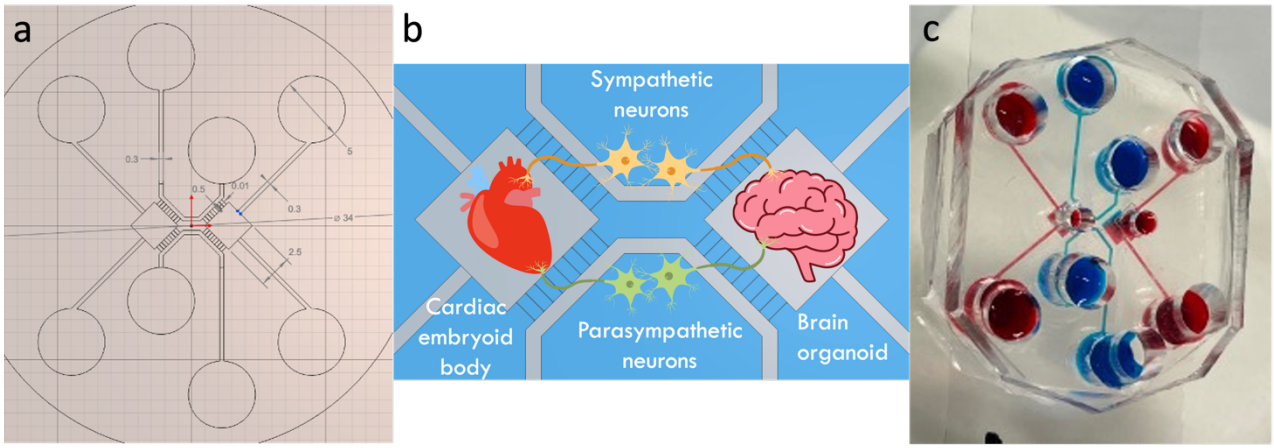

Figure 9: **Design of the generation 2.1 heart-brain axis chip.** a) Solidworks sketch with characteristic dimensions. b) Schematic of cell culture on the heart-brain axis chip. c) The PDMS chip on a coverslip with different colour dyes.

SIMULATIONS WITH COLOUR DYE INDICATE MEDIA MIXING ON CHIP

The microchannels were expected to allow for mixing in-between the compartments of the different media. Since exposure to different media can affect differentiation in the chip, it was estimated how much mixing of the media would occur during normal culture conditions within the compartments. Different colors of food dye were added to the different compartments and the chip was placed on a rocker to simulate culture conditions for 72 hours. Afterwards the liquids were aspirated from the reservoirs and absorption values for the wavelengths 520 nm and 630 nm were measured. These absorption values were related to a calibration curve to obtain estimated values for dye concentrations. After 72 hours on the rocker the initially blue neuronal reservoirs contained 27.8% ± 0.2% red dye and the initially red 3D culture reservoirs contained 26.9% ± 0.2% blue dye. However, the chips did not have any cell cultures in them potentially blocking mixing through the microchannels.

MICROCHANNELS CONTROL LOCALIZATION OF NEURONAL CULTURES

For on-chip culture, the localization of neuronal cell bodies in the neuronal compartment and the extension of neurites into the 3D culture compartments were expected. It was anticipated that the CM medium in the 3D culture compartment would exert an inhibitory effect on neurite outgrowth in comparison to conditions with ANS medium. However, it was expected that neurites would still establish direct connections with cEBs. Two separate PMMA molds were obtained using the same micro milling method and were used for chip fabrication. Neurons at day 18 of differentiation and cEBs at day 14 of differentiation were seeded on the same day in the chips and cultured for 10 and 20 days.

Immunofluorescent images showed more neurite outgrowth into the 3D culture compartment containing ANS medium on chips fabricated with mold 1 compared to on chips fabricated with mold 2 (Figure 10). A difference between molds was not expected since no differences in microchannel milling was designed. Neurites were seen growing wider than the designed microchannels and cell nuclei were seen in the 3D culture compartments in mold 1 chips but not in mold 2 chips. This suggested that cells had migrated through the microchannels in mold 1 chips. Quantification and comparison of nuclei in the 3D culture compartments could not be done since DAPI channel results were lost, but results would have been of importance for defining cell localization control of microchannels. Neurite growth into the compartments containing cEBs with CM medium was found to be less compared to compartments with only ANS medium (Figure 10). Subsequently, NKX2.5-GFP expressing cEBs did not form direct connections with neurites extending from the microchannels. To enhance chances of neurite-cEB connections in future experiments the media switch to CM media and addition of cEBs should be done at later timepoints on the chip, since the growth of the neurites is then established further into the 3D culture compartment.

On chip seeded cEBs showed NKX2.5-GFP expression and signs of contraction on day 10 (Supplementary Figure 6). This supports the expectation that the perfusion through the 3D culture compartment would improve culture conditions by reducing theorized nutrient deficiency. One cEB was seen blocking a perfusion channel, potentially being sucked into it (Supplementary Figure 6). Creating a delta plan (widening of the channel) for perfusion into the compartment instead of a thin opening this complication could be eliminated. Maturation on the chip past 20 days was compromised due to clogging of the neuronal compartment caused by cell aggregation (Supplementary Figure 7). This caused neurons to retreat from the middle of the compartments. A wider compartment should prevent clogging through aggregation. Neurons on mold 2 chip showed an increased amount of neurite outgrowth in an ANS medium containing 3D culture compartment at day 20 compared to mold 2 chips on day 10 (Figure 10). Nuclei were seen at the end of the microchannel indicating that in mold 2 chips cell migration through the microchannels was possible (Figure 10). The microfabricated chips did not fully succeed in localizing all cell bodies behind the microchannels, but these results do show that the microchannels did control the localization of neuronal cell bodies. Mold 2 chips exhibited superior control, localizing neuronal cell bodies outside the 3D compartment for 20 days, compared to Mold 1 chips (10 days). Hence, Mold 2 chips are preferred for future experiments.

Repeating the fabrication of the chips failed several times due to improper PDMS to glass bonding and alignment of reservoirs onto glass coverslips. The design was too wide for easy manual addition onto coverslips, 23 mm and 24 mm respectively. The rough milling on larger surfaces of the chip likely reduced contact of PDMS to glass. A thinner design and smoother milling finishing would improve the reproducibility of chip fabrication.

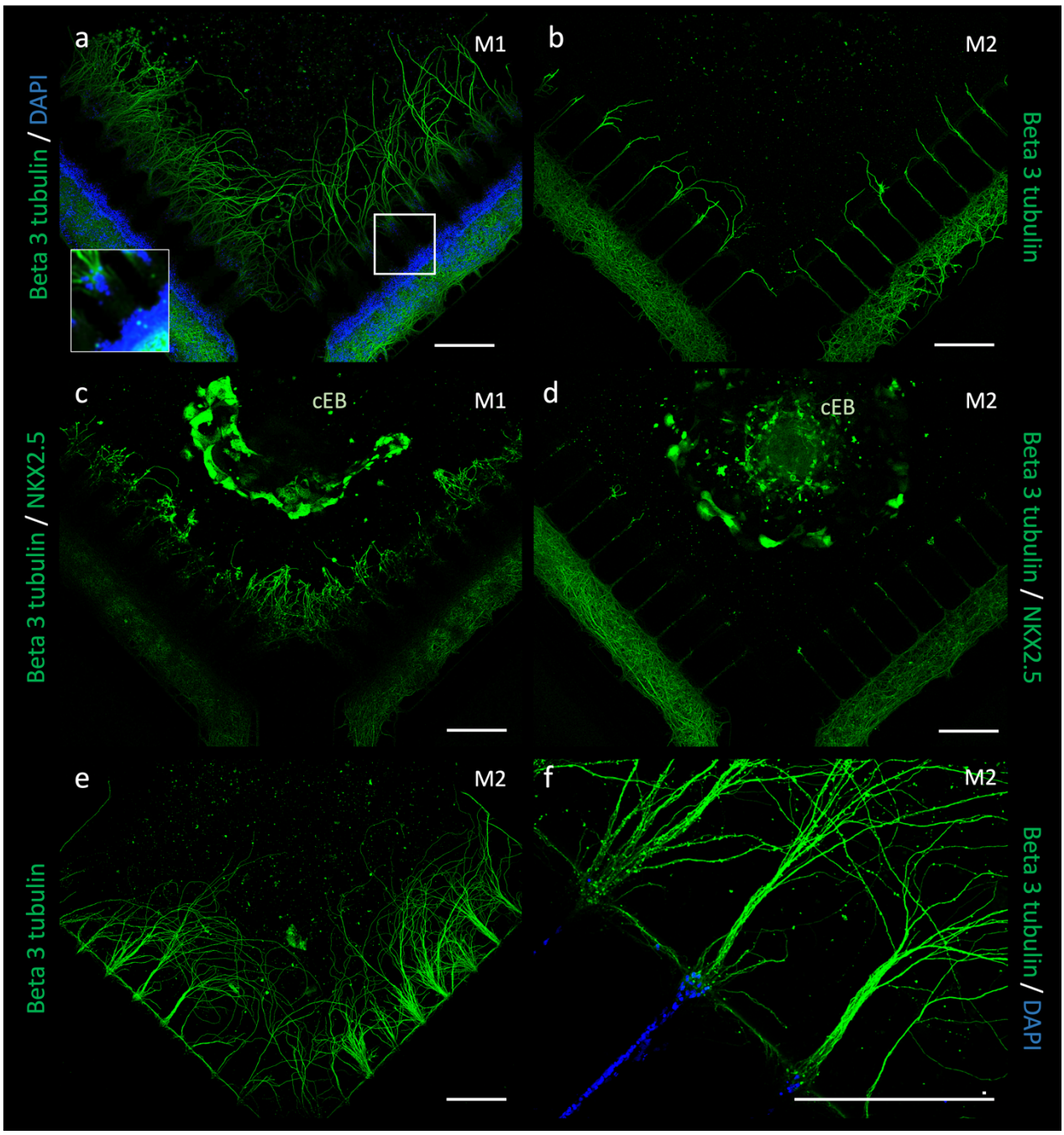

Figure 10: **Neuronal localization on the heart-brain axis chips visualized with B3-Tubulin.** a,b) Neurite outgrowth patterns into compartment containing autonomic nervous system (ANS) medium at day 10. c,d) Neurite outgrowth patterns into compartment containing cardiomyocyte maintenance (CM) medium and an NKX2.5-GFP expressing cEB at day 10. a) Neuronal localization with DAPI staining and zoom on microchannel. e,f) Neurite outgrowth patterns into compartment containing ANS medium at day 20. f) Detail image on microchannel with DAPI staining. (M1 = mold 1 fabricated chip, M2 = mold 2 fabricated chip, scalebar = 500µm)

GENERATION 2.2 (G2.2) CHIP USED IN LONG TERM NEURONAL MATURATION

In the design of the heart-brain axis chip generation 2.2 (G2.2) complications from G2.1 were aimed to be solved. Long term maturation of neurons on chip would be improved through an increase in width of the neuronal compartments, from 300 µm to 800 µm wide, allowing for larger neuronal aggregate formation without clogging of the compartments (Figure 11). Perfusion blockage in the 3D culture compartments would be negated through widening of the perfusion channels into the compartment. The general design of the chip was adjusted to better fit onto coverslips and PMMA mold surfaces were milled twice with an additional inverse milling path to create smoother surfaces. These steps would give easier fabrication and better reproducibility. To obtain control on neuron localization molds were made with similar milling paths for the microchannels as used in G2.1 mold 2.

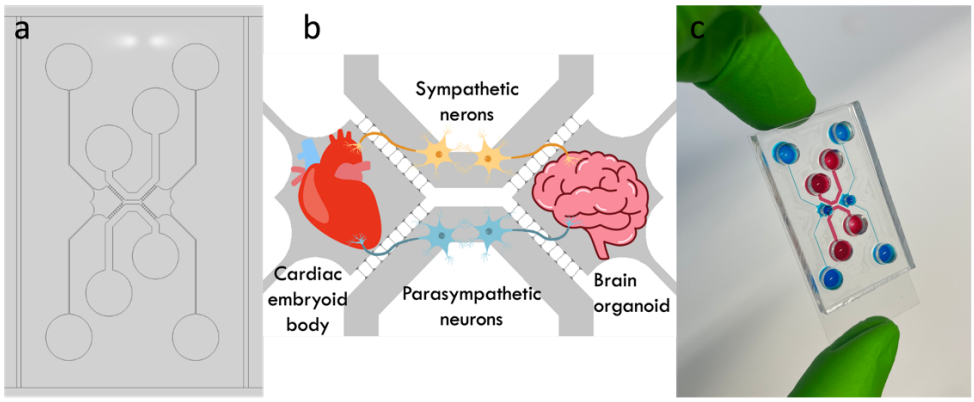

Figure 11: **Design of the generation 2.2 heart-brain axis chip.** a) A Solidworks sketch of the new layout. b) Updated schematic of cell culture on the heart-brain axis chip. c) The PDMS chip on a coverslip with different colour dyes.

Fabrication of the chips went without any complications. Neurons at day 18 of differentiation were seeded on the chip and matured for 30 days on chip (Figure 12). The neurons showed neuronal aggregates and neurite bundles between the aggregates, morphological characteristics for mature neuronal cultures[24][25]. The neurites did sprout towards microchannel openings, but the microchannels were closed. The variation in microchannel functionality over the different molds indicated that current micro milling methods are suboptimal for obtaining 10 µm x 10 µm microchannel sizes. The dimensions needed for mold fabrication are close to the limits of micro milling[42]. Other methods like stereolithography offer higher precision and accuracy of these smaller structures[42], [43]. Stereolithography would allow for the optimization on microchannel sizes for the heart-brain axis chip due to the control on these sizes. Variations in amount, directory, thickness, and length of the neurite outgrowth could be controlled for either optimal innervation or to simulate uneven innervation on chip.

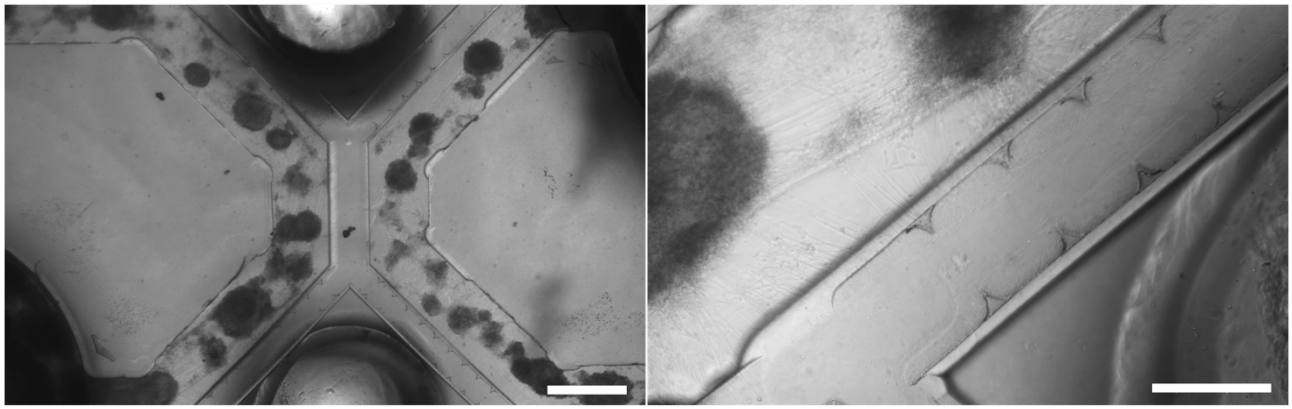

Figure 12: **Long term neuronal maturation of 30 days on chip.** Left) Neuronal aggregates through-out the neuronal compartment. (scalebar = 1mm) Right) Neurite bundles between the aggregates and towards closed microchannel openings. (scalebar = 300µm)

GENERATION 2.3 (G2.3)

The design of the heart-brain axis chip generation 2.3 (G2.3) did not differ from the G2.2 design. The design aims to improve on complications of the G2.1 chip and improve on the resolution of the G2.2 chip. Improving on the resolution of the chip would be achieved through the production of SU-8 stereolithography fabrication.

CELL LOCALIZATION ALLOWED FOR DISTINGUISHING CARDIAC EMBRYOID BODY GROWN NEURITES

SU-8 is a negative photoresist which can be spin coated at different speeds to alter the thickness. Through exposure of UV light, the resist is hardened, but overexposure broadens the structure exposed to UV light due to scattering. The fabrication of SU-8 microchannel structures with heights of 10 or 15 µm and widths of 8 µm or wider were to be fabricated. The variation in different shapes and sizes were expected to show differences in control on localization of neuronal cell bodies and differences in neurite outgrowth. The 8 by 10 µm and the 8 by 16 µm structures were expected to localize cell bodies in the neuronal compartment, with a higher amount of neurite outgrowth for the larger structure. The wider structure with 10 µm in height was expected to control the localization of cell bodies, but not localize completely in the neuronal compartment, since 10 µm was reported to be the minimum dimension to hold back neuronal cell bodies[41]. To obtain neuron to cardiac connections with this controlled cell localization cEBs would be co-cultured for 7 days in the compartment where neurite outgrowth has been initiated during the preceding 10 days of monoculture.

Developed molds were measured to have the following widths and heights for microchannels, mold 1 had 12 by 10 µm, mold 2 had 8 by 10 µm, mold 3 had 8 by 16 µm. Overexposure on mold 1 did result in wider microchannels. Mold 2 was measured to be higher, but these height measurements were performed on resolution markers at the edges of the wafer and might not be representable for the entire wafer.

Neurite outgrowth and neuronal cell body localization was per mold used unique (Figure 13). Comparing neurite outgrowth into the 3D culture compartment, mold 1 chips displayed the most extensive growth, with millimeter-long neurites from microchannel endings. Mold 2 chips showed less extensive outgrowth of about 500 µm, while mold 3 chips exhibited only neurite buds. The relatively large outgrowth in mold 1 chips may result from having up to 100 neuronal cell bodies at microchannel ends (manually counted) with additional cells in the channels. Mold 2 chips had about 15 neuronal cell bodies in the microchannels (manually counted), and Mold 3 chips also contained neuronal cell bodies in microchannels. That the microchannels with the smallest dimension would have the best effect on localizing cell bodies was expected. However, that the microchannels with the largest dimension did not have the highest neurite outgrowth was unexpected. Potentially the high width to height ratio of the channel allowed to be pressed closed during PDMS-glass bonding. To prevent this higher curing agent to polymer ratios for PDMS production should be used to create stiffer chips.

When looking at the B3-Tubulin expression in the coculture conditions, expression can be seen in high amounts and far away from the neuronal compartments on all mold type chips. Expression characterized and located like this was not expected. Mold 3 chips which in control conditions only formed neurite budding, were seen with an almost full neurite mesh around the entire cEB. Repetition of this experiment with multiple timepoints would give more information on how this developed or whether a mistake occurred during cEB seeding. B3-Tubulin expression and neural crest cells were found in EBs differentiated with heterogeneous cell populations in literature[44], [45]. These findings suggest that the neurite outgrowth on the cEB might be due to neuron-like differentiated cells from within the cEB. Variation in cEB differentiation might explain why something similar was not previously found within the heart-brain axis project.

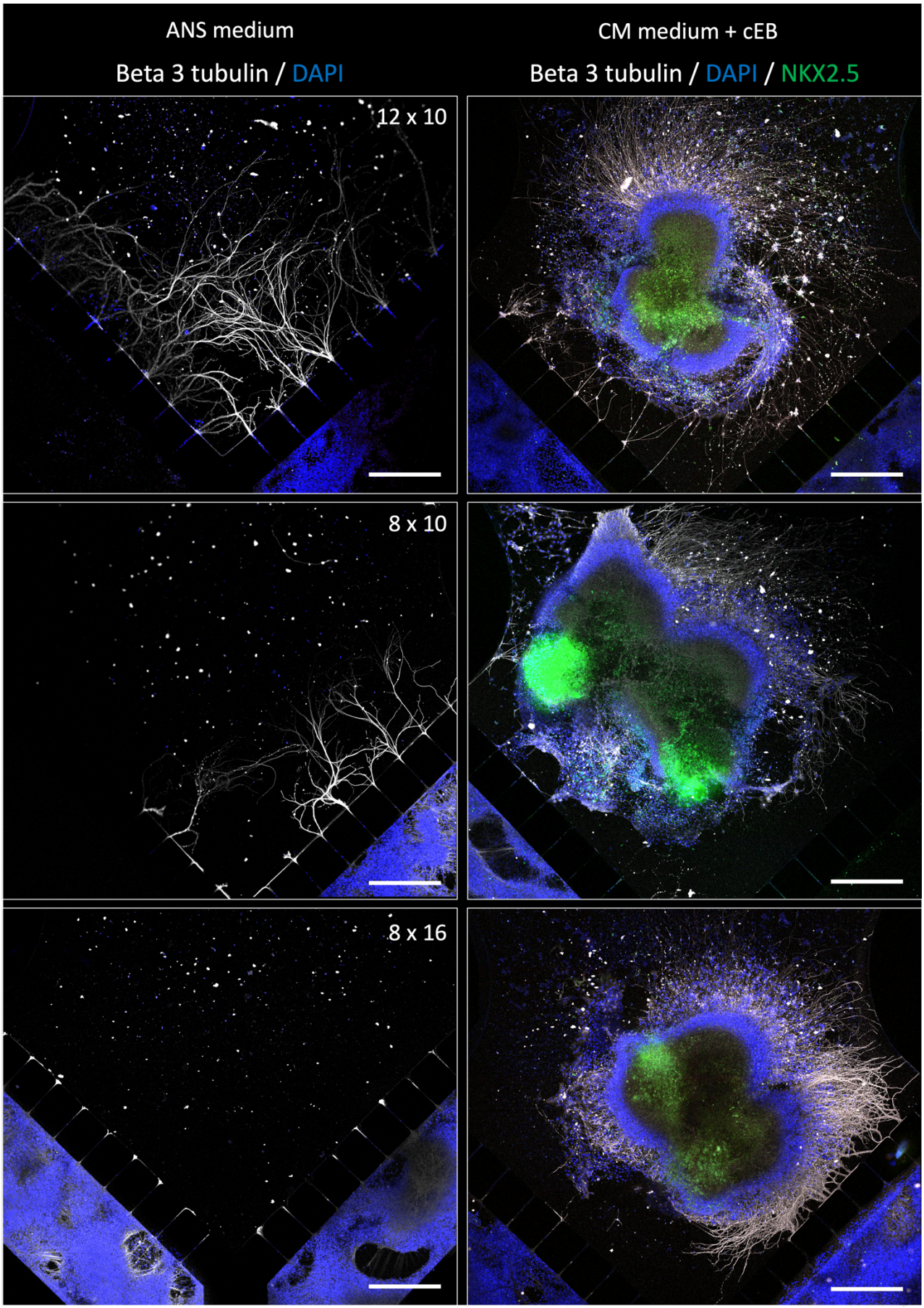

Figure 13: **Neuronal localization and neuron-cardiac connections on the heart-brain axis chip.** Left panel shows neuronal monoculture at 17 days on chip. Right panel shows cardiac embryoid bodies with direct neuronal connections at 10 days of coculture. From top to bottom 3 panels are shown with the dimensions of the microchannels written in the panel, e.g. 12 x 10 µm w x h. (scalebar = 500µm)

CALCIUM IMAGING SHOWS EXCITABLE NEURONS ON CHIP

Calcium imaging was not successful in piloting work of the heart-brain axis on chip since the staining could not perfuse through the chip to stain the cultures. The cultures are expected to be stained, showing visible structures and through excitation of the neurons with KCl solution the neurons should show increased signal. Since newer generations of the chip allow for better perfusion, the stainings and excitation were expected to work accordingly.

Neurons were matured for 32 days on a G2.2 chip and matured for 20 days on a G2.1 chip before being used for staining (Figure 14). The chip was stained successfully, highlighting the aggregated neurons with neurite bundles inside the chip. Upon addition of the KCl solution into the reservoir, intensity of signal slowly raised which was comparable to results seen in literature[24](Supplemental Figure 8). Intensity of the fluorescent signal after excitation for regions of interest (ROIs) 1, 2, and 3 throughout the compartment were measured. It could be seen that that ROI1 and subsequently ROI2 had an increase in fluorescent signal. This means that the calcium imaging and excitation worked as expected. It is however not clear with this data whether the timed difference in excitation of ROI2 compared to ROI1 was due to propagation of the signal through the neurons or through diffusion and or perfusion of KCl concentrations. Experiments with a blockage for perfusion and diffusion should be performed to determine this. However, since this staining was done on G2.2 which does not allow for neurite formation through the microchannels, this could not be done.

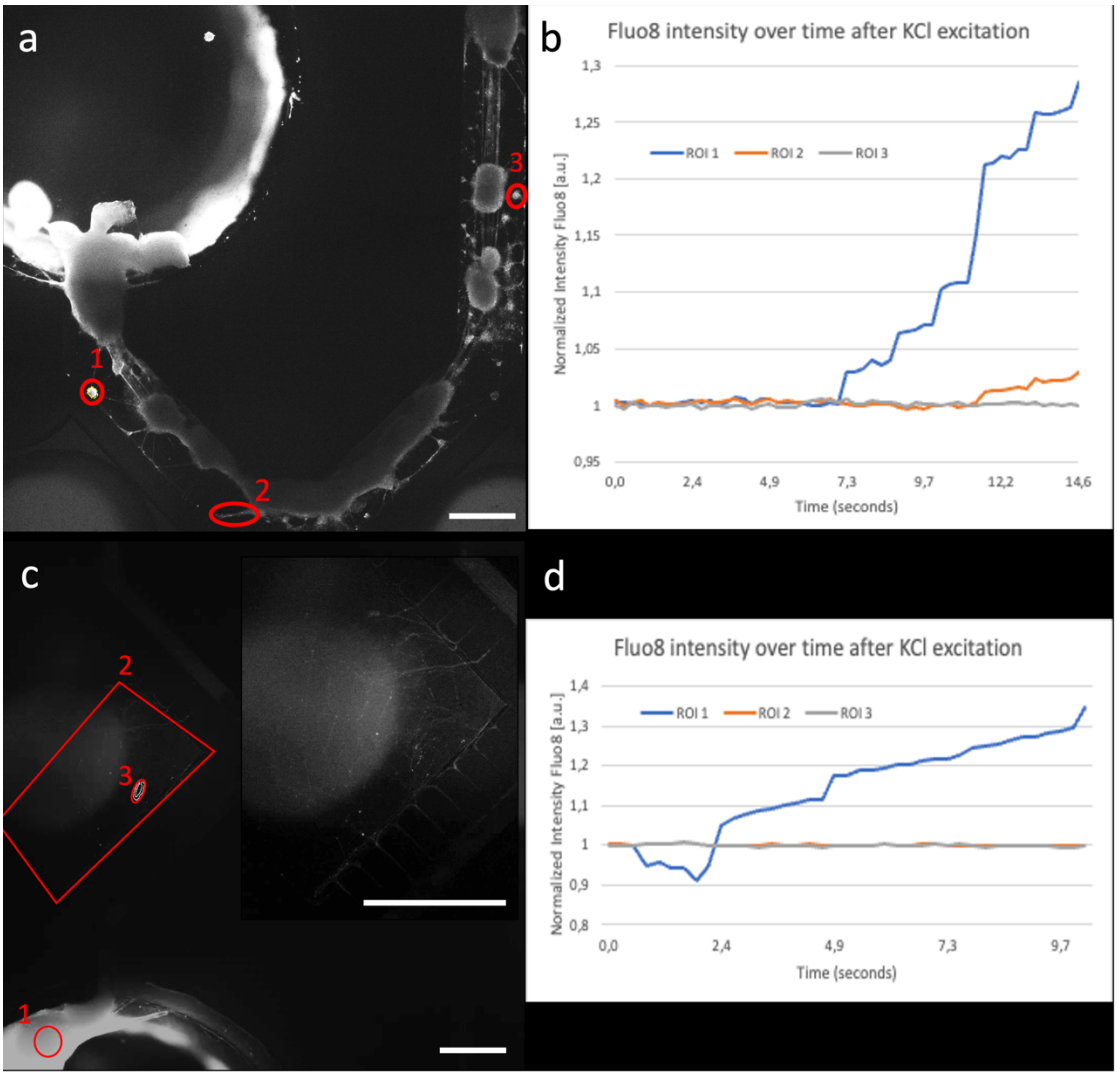

Figure 14: Calcium imaging on the heart-brain chips. a) Grayscale image of successfully stained neurons on chip with chosen ROIs. b) Fluorescent intensity over time of ROIs in “a” after KCl excitation. c) Grayscale image of successfully stained neurites on chip. d) Fluorescent intensity over time of ROIs in “c” after KCl excitation. (scalebar = 1mm)

In the G2.1 chip the staining was not successful for the neuronal compartment except for in the reservoir (Figure 14). Neurites in the 3D cell culture compartment did stain as expected. Said regions were chosen as ROI and intensity was measured. The KCl solution was added to the reservoir and directly impacted tissue showed an increase in fluorescent signal (Figure 14). ROIs in the 3D cell compartment did not show any significant increase in intensity. The time frame of when this was measured was however short. The distance from ROI1 to ROI2 in G2.2 was about 2.5mm and the signal took (via either perfusion or propagation) 3.5 seconds. The distance from ROI1 to ROI3 in G2.1 was 4.5mm, meaning that with a similar speed the signal would take at least 6.3 seconds to reach ROI3 after ROI1 excitation. The potential first sign would then have occurred at about 9 seconds into the graph, which is late. A recommendation on performing similar experiments for future chips would be to use longer recording timeframes.

FUTURE OUTLOOK

The future of the heart-brain axis on chip is still new with multiple pathways to be explored. Possibilities in disease model development, therapy development, but also fundamental developmental biology are open.

The G2.3 heart-brain axis on chip currently allows for controlled localization of neuronal cells and with this variable under control, short term future goals could be set for the chemical influencing of innervation. Using NGF or Sema3a on the neural-cardiac connections, the amount and the patterning of innervation can be changed to mimic disease like states. Hyperinnervation and unbalanced patterning both are known to induce arrythmia[14]. Analysis of calcium imaging patterns on the cEB could allow for characterization of these different pathologies.

Other important short-term aims should be set on the validation of the neural-cardiac connections. Further research into the neurotransmitters secreted by the ANS differentiations on chip will be crucial for the substantiation of the mechanisms for cardiac function regulation. Measured concentrations of neurotransmitters secreted into the cEB environment and characterization of the cEBs functionality will be a foundation for future cardiac regulating mechanism.

Potential excursions into electrical stimulation of neuronal cells could allow for the controlled release of neurotransmitters, in turn regulating cardiac functioning. Electrical stimulation of ANS cells showed a modulating effect on heartbeat frequency in rat primary cells[27]. The electrical stimulation of ANS cells innervating cEB, would offer great possibilities in disease modeling. Sending erratic signals to model for stroke, hyperactivation of sympathetic cells for long durations to model for chronic stress or chronic inflammation, decreased[2], [8]. Besides disease modelling, electrical stimulation was shown to enhance both neuronal and cardiac differentiation[46], [47]. The substrate bound culture of ANS differentiated cells make it an easy target to stimulate or record non-stop real-time with integrated electrodes on chip. In the future even 3D multi electrode arrays could also allow for read-outs of the 3D cultures[48].

The ability of hPSCs-derived ANS cells to grow neurite bundles in three dimensions, climbing up on wallsubstrates or 3D cell cultures makes the cell model multi-deployable. Both 2D cultures as well as 3D cell cultures could be co-cultured with these cells. Combining for example these cells with micro engineered heart tissues could allow for the innervating neurite bundles to hang onto beating suspended tissues, regulating the beating characteristics. This would even make way for the direct quantification of the effect of said innervation. Furthermore, since the ANS is involved in many different organs, like the kidneys, the liver, the lungs, etc. you could create a model for many more axis. Also, the heart-brain axis on chip would function for various 3D or 2D structure cultures which require innervation.

The heart-brain axis will still require a lot more development to be able to mimic the feedback mechanisms behind the baroreceptor reflex, but the first connections are already made.

CONCLUSIONS

In conclusion, this thesis aimed to address the critical need for a model representing the intrinsic axis between the brain and the heart for disease modeling. The primary goal was to develop a model capable of mimicking the influence of the brain on heartbeat regulation through the innervation of autonomic nervous cells using human pluripotent stem cells (hPSCs) on a microfluidic chip. The project unfolded in several key phases.

Firstly, various cell differentiations crucial for simulating the brain's impact on heartbeat regulation were successfully achieved from hESCs, including cardiac embryoid bodies (cEB), brain organoids (BO), and vagal nerve differentiations. To introduce a counter effect on vagal heartbeat regulation, a sympathetic nerve-like cell differentiation from hESCs was conducted and described as morphologically distinct from vagal nerve-like cells. Expression for tyrosine hydroxylase (TH) was not found in both hESC-derived sympathetic nerve-like cells and SH-SY5Y cells exposed with either retinoic acid (RA) or dbcAMP, indicating a non-functioning TH-antibody.

Secondly, biological research supporting the process optimization of the project was performed. Reducing the size of mature BOs to easy seeding into microfluidic chips was tested by seeding various initial densities, but this was found ineffective. Cryopreservation of beating cEBs, for the facilitation of simplified planning for the project, was found feasible with cEBs contracting and NKX2.5-GFP/ACTN2-mRuby positive after thawing. Simulating potential on chip conditions by exposing neuron precursor cells to cardiomyocyte maintenance (CM) media did not cause loss of neurite formation.

Lastly, a microfluidic chip for the controlled co-culture of hPSC-derived cEBs, BOs and nerve cells was expanded upon and optimized. To better distinguish these cultures during characterization and analysis, the controlled localization of these cells on chip was achieved. By incorporating medium reservoirs directly onto the chip and implementing hydrostatic perfusion across four distinct compartments, we enhanced chip handling, addressed issues related to nutrient deficiency and live cell staining inefficiency, and allowed accommodation for an additional cell type.

This comprehensive approach not only contributes to advancing the understanding of the heart-brain axis but also provides a robust foundation for disease modeling and therapeutic research in the context of cardiac regulation influenced by neural connections.

REFERENCES

[1] P. Tahsili-Fahadan and R. G. Geocadin, "Heart–Brain Axis," *Circ Res*, vol. 120, no. 3, pp. 559–572, Feb. 2017, doi: 10.1161/CIRCRESAHA.116.308446.

[2] A. Silvani, G. Calandra-Buonaura, R. A. L. Dampney, and P. Cortelli, "Brainheart interactions: physiology and clinical implications," *Philosophical Transactions of the Royal Society A: Mathematical, Physical and Engineering Sciences*, vol. 374, no. 2067, May 2016, doi: 10.1098/RSTA.2015.0181.

[3] A. M. D. Végh *et al.*, "Part and Parcel of the Cardiac Autonomic Nerve System: Unravelling Its Cellular Building Blocks during Development," *Journal of Cardiovascular Development and Disease 2016, Vol. 3, Page 28*, vol. 3, no. 3, p. 28, Sep. 2016, doi: 10.3390/JCDD3030028.

[4] L. Fedele and T. Brand, "The Intrinsic Cardiac Nervous System and Its Role in Cardiac Pacemaking and Conduction," *Journal of Cardiovascular Development and Disease 2020, Vol. 7, Page 54*, vol. 7, no. 4, p. 54, Nov. 2020, doi: 10.3390/JCDD7040054.

[5] R. Gordan, J. K. Gwathmey, and L.-H. Xie, "Autonomic and endocrine control of cardiovascular function," *World J Cardiol*, vol. 7, no. 4, p. 204, Apr. 2015, doi: 10.4330/WJC.V7.I4.204.

[6] R. A. L. Dampney, "Central neural control of the cardiovascular system: Current perspectives," *Adv Physiol Educ*, vol. 40, no. 3, pp. 283–296, 2016, doi: 10.1152/advan.00027.2016.

[7] I. M. Salman, "Major Autonomic Neuroregulatory Pathways Underlying Short- and Long-Term Control of Cardiovascular Function," *Curr Hypertens Rep*, vol. 18, no. 3, pp. 1–18, Mar. 2016, doi: https://doi.org/10.1007/s11906-016-0625-x.

[8] O. Oladiran and I. Nwosu, "Stroke risk stratification in atrial fibrillation: a review of common risk factors," *J Community Hosp Intern Med Perspect*, vol. 9, no. 2, p. 113, Mar. 2019, doi: 10.1080/20009666.2019.1593781.

[9] F. Seifert *et al.*, "Neuroanatomical correlates of severe cardiac arrhythmias in acute ischemic stroke," *J Neurol*, vol. 262, no. 5, pp. 1182–1190, May 2015, doi: 10.1007/S00415-015-7684-9.

[10] F. Pelliccia, J. C. Kaski, F. Crea, and P. G. Camici, "Pathophysiology of Takotsubo Syndrome," *Circulation*, vol. 135, no. 24, pp. 2426–2441, Jun. 2017, doi: 10.1161/CIRCULATIONAHA.116.027121.

[11] J. S. Floras and P. Ponikowski, "The sympathetic/parasympathetic imbalance in heart failure with reduced ejection fraction," *Eur Heart J*, vol. 36, no. 30, pp. 1974–1982, Aug. 2015, doi: 10.1093/EURHEARTJ/EHV087.

[12] A. Sgoifo, L. Carnevali, M. D. L. A. Pico Alfonso, and M. Amore, "Autonomic dysfunction and heart rate variability in depression," *Stress*, vol. 18, no. 3, pp. 343–352, May 2015, doi: 10.3109/10253890.2015.1045868.

[13] M. A. De Vilhena Toledo and L. F. Junqueira, "Cardiac sympathovagal modulation evaluated by short-term heart interval variability is subtly impaired in Alzheimer's disease," *Geriatr Gerontol Int*, vol. 8, no. 2, pp. 109–118, Jun. 2008, doi: 10.1111/J.1447-0594.2008.00456.X.

[14] K. Fukuda, H. Kanazawa, Y. Aizawa, J. L. Ardell, and K. Shivkumar, "Cardiac Innervation and Sudden Cardiac Death," *Circ Res*, vol. 116, no. 12, pp. 2005–2019, Jun. 2015, doi: 10.1161/CIRCRESAHA.116.304679.

[15] Y. Hou, Q. Zhou, and S. S. Po, "Neuromodulation for cardiac arrhythmia," *Heart Rhythm*, vol. 13, no. 2, pp. 584–592, Feb. 2016, doi: 10.1016/J.HRTHM.2015.10.001.

[16] Y. Shi, H. Inoue, J. C. Wu, and S. Yamanaka, "Induced pluripotent stem cell technology: a decade of progress," *Nature Reviews Drug Discovery 2016 16:2*, vol. 16, no. 2, pp. 115–130, Dec. 2016, doi: 10.1038/NRD.2016.245.

[17] C. M. Leung *et al.*, "A guide to the organ-on-a-chip," *Nature Reviews Methods Primers 2022 2:1*, vol. 2, no. 1, pp. 1–29, May 2022, doi: 10.1038/s43586-022-00118-6.

[18] E. S. Ng, R. Davis, E. G. Stanley, and A. G. Elefanty, "A protocol describing the use of a recombinant protein-based, animal product-free medium (APEL) for human embryonic stem cell differentiation as spin embryoid bodies," *Nature Protocols 2008 3:5*, vol. 3, no. 5, pp. 768–776, Apr. 2008, doi: 10.1038/NPROT.2008.42.

[19] V. Schwach, C. Cofiño-Fabres, S. A. Ten Den, and R. Passier, "Improved Atrial Differentiation of Human Pluripotent Stem Cells by Activation of Retinoic Acid Receptor Alpha (RARα)," *J Pers Med*, vol. 12, no. 4, Apr. 2022, doi: 10.3390/JPM12040628/S1.

[20] R. Shinnawi *et al.*, "Monitoring Human-Induced Pluripotent Stem Cell-Derived Cardiomyocytes with Genetically Encoded Calcium and Voltage Fluorescent Reporters," *Stem Cell Reports*, vol. 5, no. 4, pp. 582–596, Oct. 2015, doi: 10.1016/J.STEMCR.2015.08.009.

[21] M. C. Ribeiro *et al.*, "A cardiomyocyte show of force: A fluorescent alpha-actinin reporter line sheds light on human cardiomyocyte contractility versus substrate stiffness," *J Mol Cell Cardiol*, vol. 141, pp. 54–64, Apr. 2020, doi: 10.1016/J.YJMCC.2020.03.008.

[22] W. Dou *et al.*, "Microengineered platforms for characterizing the contractile function of in vitro cardiac models," *Microsystems & Nanoengineering 2022 8:1*, vol. 8, no. 1, pp. 1–22, Feb. 2022, doi: 10.1038/s41378-021-00344-0.

[23] J. Luo and P. Li, "Human pluripotent stem cell-derived brain organoids as in vitro models for studying neural disorders and cancer," *Cell & Bioscience 2021 11:1*, vol. 11, no. 1, pp. 1–17, May 2021, doi: 10.1186/S13578-021-00617-1.

[24] F. Fattahi *et al.*, "Deriving human ENS lineages for cell therapy and drug discovery in Hirschsprung disease," *Nature 2016 531:7592*, vol. 531, no. 7592, pp. 105–109, Feb. 2016, doi: 10.1038/nature16951.

[25] K. Saito-Diaz, H. F. Wu, and N. Zeltner, "Autonomic Neurons with Sympathetic Character Derived From Human Pluripotent Stem Cells," *Curr Protoc Stem Cell Biol*, vol. 49, no. 1, p. e78, Jun. 2019, doi: 10.1002/CPSC.78.

[26] A. Winbo, S. Ramanan, E. Eugster, S. Jovinge, J. R. Skinner, and J. M. Montgomery, "Functional coculture of sympathetic neurons and cardiomyocytes derived from human-induced pluripotent stem cells," *Am J Physiol Heart Circ Physiol*, vol. 319, no. 5, pp. H927–H937, Oct. 2020, doi: 10.1152/AJPHEART.00546.2020.

[27] K. Oiwa, K. Shimba, T. Numata, A. Takeuchi, K. Kotani, and Y. Jimbo, "A device for co-culturing autonomic neurons and cardiomyocytes using micro-fabrication techniques," *Integrative Biology*, vol. 8, no. 3, pp. 341–348, Mar. 2016, doi: 10.1039/C5IB00273G.

[28] L. S. Koch, D. C. Buentello, and K. Broersen, "Robust Tissue Fabrication for Long-Term Culture of iPSC-Derived Brain Organoids for Aging Research," *JoVE (Journal of Visualized Experiments)*, vol. 2023, no. 195, p. e64586, May 2023, doi: 10.3791/64586.

[29] H. F. Wu and N. Zeltner, "Efficient differentiation of postganglionic sympathetic neurons using human pluripotent stem cells under feeder-free and chemically defined culture conditions," *Journal of Visualized Experiments*, vol. 2020, no. 159, pp. 1–14, May 2020, doi: 10.3791/60843.

[30] A. Janesick, S. C. Wu, and B. Blumberg, “Retinoic acid signaling and neuronal differentiation,” *Cellular and Molecular Life Sciences*, vol. 72, no. 8, pp. 1559–1576, Jan. 2015, doi: 10.1007/S00018-014-1815-9/FIGURES/2.

[31] H. F. Wu and N. Zeltner, “Overview of Methods to Differentiate Sympathetic Neurons from Human Pluripotent Stem Cells,” *Curr Protoc Stem Cell Biol*, vol. 50, no. 1, p. e92, Sep. 2019, doi: 10.1002/CPSC.92.

[32] J. Kovalevich and D. Langford, “Considerations for the Use of SH-SY5Y Neuroblastoma Cells in Neurobiology,” *Methods Mol Biol*, vol. 1078, p. 9, 2013, doi: 10.1007/978-1-62703-640-5_2.

[33] S. P. Presgraves, T. Ahmed, S. Borwege, and J. N. Joyce, “Terminally differentiated SH-SY5Y cells provide a model system for studying neuroprotective effects of dopamine agonists,” *Neurotox Res*, vol. 5, no. 8, pp. 579–598, 2004, doi: 10.1007/BF03033178.

[34] T. Kume *et al.*, “Dibutyryl cyclic AMP induces differentiation of human neuroblastoma SH-SY5Y cells into a noradrenergic phenotype,” *Neurosci Lett*, vol. 443, no. 3, pp. 199–203, Oct. 2008, doi: 10.1016/J.NEULET.2008.07.079.

[35] T. Neutelings, C. A. Lambert, B. V. Nusgens, and A. C. Colige, “Effects of Mild Cold Shock (25°C) Followed by Warming Up at 37°C on the Cellular Stress Response,” *PLoS One*, vol. 8, no. 7, Jul. 2013, doi: 10.1371/JOURNAL.PONE.0069687.

[36] L. van den Brink *et al.*, “Cryopreservation of human pluripotent stem cell-derived cardiomyocytes is not detrimental to their molecular and functional properties,” *Stem Cell Res*, vol. 43, p. 43, Mar. 2020, doi: 10.1016/j.scr.2019.101698.

[37] X. Li, R. Krawetz, S. Liu, G. Meng, and D. E. Rancourt, “ROCK inhibitor improves survival of cryopreserved serum/feeder-free single human embryonic stem cells,” *Hum Reprod*, vol. 24, no. 3, pp. 580–589, 2009, doi: 10.1093/HUMREP/DEN404.

[38] L. Cao, L. Schoenmaker, S. A. Ten Den, R. Passier, V. Schwach, and F. J. Verbeek, “Automated Sarcomere Structure Analysis for Studying Cardiotoxicity in Human Pluripotent Stem Cell-Derived Cardiomyocytes,” *Microscopy and Microanalysis*, vol. 29, no. 1, pp. 254–264, Feb. 2023, doi: 10.1093/MICMIC/OZAC016.

[39] D. A. Elliott *et al.*, “NKX2-5eGFP/w hESCs for isolation of human cardiac progenitors and cardiomyocytes,” *Nature Methods 2011 8:12*, vol. 8, no. 12, pp. 1037–1040, Oct. 2011, doi: 10.1038/nmeth.1740.

[40] D. C. Buentello, L. S. Koch, G. Trujillo-De Santiago, M. M. Alvarez, and K. Broersen, “Use of standard U-bottom and V-bottom well plates to generate neuroepithelial embryoid bodies,” *PLoS One*, vol. 17, no. 5, p. e0262062, May 2022, doi: 10.1371/JOURNAL.PONE.0262062.

[41] R. Habibey, J. E. Rojo Arias, J. Striebel, and V. Busskamp, “Microfluidics for Neuronal Cell and Circuit Engineering,” *Chem Rev*, vol. 122, no. 18, pp. 14842–14880, Sep. 2022, doi: 10.1021/ACS.CHEMREV.2C00212/ASSET/IMAGES/LARGE/CR2C00212_0006.JPEG.

[42] D. J. Guckenberger, T. E. De Groot, A. M. D. Wan, D. J. Beebe, and E. W. K. Young, “Micromilling: A method for ultra-rapid prototyping of plastic microfluidic devices,” *Lab Chip*, vol. 15, no. 11, p. 2364, Jun. 2015, doi: 10.1039/C5LC00234F.

[43] A. G. Niculescu, C. Chircov, A. C. Bîrcă, and A. M. Grumezescu, “Fabrication and Applications of Microfluidic Devices: A Review,” *Int J Mol Sci*, vol. 22, no. 4, pp. 1–26, Feb. 2021, doi: 10.3390/IJMS22042011.

[44] R. H. Mennen, N. Hallmark, M. Pallardy, R. Bars, H. Tinwell, and A. H. Piersma, “Molecular neural crest cell markers enable discrimination of organophosphates in the murine cardiac embryonic stem cell test,” *Toxicol Rep*, vol. 8, pp. 1513–1520, Jan. 2021, doi: 10.1016/J.TOXREP.2021.07.017.

[45] R. H. Mennen, N. Hallmark, M. Pallardy, R. Bars, H. Tinwell, and A. H. Piersma, "Gene regulation by morpholines and piperidines in the cardiac embryonic stem cell test," *Toxicol Appl Pharmacol*, vol. 433, p. 115781, Dec. 2021, doi: 10.1016/J.TAAP.2021.115781.

[46] S. Wang, S. Guan, C. Sun, H. Liu, T. Liu, and X. Ma, "Electrical stimulation enhances the neuronal differentiation of neural stem cells in three-dimensional conductive scaffolds through the voltage-gated calcium ion channel," *Brain Res*, vol. 1798, p. 148163, Jan. 2023, doi: 10.1016/J.BRAINRES.2022.148163.

[47] J. Li *et al.*, "Circulating re-entrant waves promote maturation of hiPSC-derived cardiomyocytes in self-organized tissue ring," *Communications Biology 2020 3:1*, vol. 3, no. 1, pp. 1–12, Mar. 2020, doi: 10.1038/s42003-020-0853-0.

[48] J. S. Choi, H. J. Lee, S. Rajaraman, and D. H. Kim, "Recent advances in three-dimensional microelectrode array technologies for in vitro and in vivo cardiac and neuronal interfaces," *Biosens Bioelectron*, vol. 171, p. 112687, Jan. 2021, doi: 10.1016/J.BIOS.2020.112687.

APPENDIX (QR)

QR code leading to a Google drive containing Supplementary Information